

# Swallow-Tailed Polycatenars: Controlling Complex Liquid Crystal Self-Assembly and Mirror Symmetry Breaking at the Lamellae-Network Cross-Over

Tino Reppe, Christian Dressel, Silvio Poppe, Alexey Eremin, and Carsten Tschierske\*

Controlling the spatial organization of  $\pi$ -conjugated molecules in soft systems is of importance for the design of new materials with application relevant optimized properties. Here, soft self-assembly of functional multi-chained  $\pi$ -conjugated 5,5'-diphenyl-2,2'-bithiophenes is investigated. Focus is on molecules with a 3,5-disubstitution pattern at one end and no or only a single chain at the other end. By elongation of the single terminal chain, a transition from lamellar phases to helical networks is observed. With lowering the temperature, the lamellar phase types change from smectic via hexatic to crystalline. In some cases, different kinds of orders are combined in a single uniform lamellar structure. Moreover, a transition from uniform (synclinic) to alternating (anticlinic) tilt in adjacent layers is observed with decreasing chain length or rising temperature, due to a change of the molecular conformation from tuning fork like to Y-shaped. For compounds terminated with a long chain, helical self-assembly of the  $\pi$ -conjugated rods in networks takes place, leading either to a racemic ( $Ia\bar{3}d$ , gyroid) or a spontaneous mirror symmetry broken ( $I23$ ) bicontinuous cubic phase and a chiral isotropic liquid phase ( $Iso_1^{[3]}$ ) as well. This work establishes rules for controlling the self-assembly of functional  $\pi$ -conjugated rods in soft matter and fluids.

molecules in soft self-organized supramolecular systems.<sup>[1,2]</sup> Extended  $\pi$ -conjugated systems are also of significant interest for application as charge carrier in organic semiconductors,<sup>[3]</sup> luminescent materials (e.g., AIEgens),<sup>[4]</sup> and for circular polarized emission in helical assemblies.<sup>[5]</sup> Therefore, tuning the organization of these  $\pi$ -conjugated rods in soft matter systems is fundamental and requires the understanding of their general design rules. Liquid crystals (LCs) are of great interest as stimuli-responsive and switchable optical materials in displays, photonics<sup>[6]</sup> and in sensor applications.<sup>[7,8]</sup> Rod-like  $\pi$ -conjugated molecules with multiple end-chains, the so-called polycatenar molecules, have received significant interests as they provide a huge variety of different LC phases ranging from lamellar (smectic, Sm) via bicontinuous cubic ( $Cub_{bi}$ ) to columnar (Col)<sup>[9–11]</sup> and even micellar cubic phases.<sup>[3]</sup> This observation has contributed to the recognition of the importance of


nano-segregation for LC phase formation and demonstrated the similarity of the fundamental self-assembly principles in lyotropic systems formed by amphiphiles, in LC phases and in the solid state morphologies of block copolymers.<sup>[12,13]</sup> Among the self-assembled structures of polycatenar molecules, the  $Cub_{bi}$  phases<sup>[14,15]</sup> received special attention because of their potential for applications, as for example in 3D conducting<sup>[16]</sup> and photonic materials,<sup>[17]</sup> being the result of their interwoven network structure (see Section 3.6).<sup>[14,18]</sup> Generally the  $Cub_{bi}$  phases are found at the transition between lamellar and columnar modes of self-assembly as a result of the developing interface curvature.<sup>[12,19–21]</sup> The most common  $Cub_{bi}$  phase is the double gyroid with space group  $Ia\bar{3}d$  and three way junctions forming two interwoven networks,<sup>[21,22]</sup> but also double diamond phases ( $Pn\bar{3}m$ ) with four-way junctions and primitive networks with six-way junctions ( $Im\bar{3}m$ ) are known.<sup>[14,19]</sup> Only recently the related single network cubic phases were found in thermotropic LCs.<sup>[23]</sup> There is also a  $Cub_{bi}$  phase with more complex triple network structure (previously designated as  $Im\bar{3}m$ ) which is only formed in systems involving rod-like units, the polycatenars being the most prominent, and different models are under discussion, as will be described in Section 3.6.<sup>[24–26]</sup> The recent discovery of helix formation, spontaneous mirror symmetry breaking, optical activity and enormous chirality

## 1. Introduction

Using sunlight as a sustainable energy source is of vital interest for the survival of the continuously growing mankind. As known from nature, efficient light-harvesting requires the aggregation and defined organization of arrays of  $\pi$ -conjugated

T. Reppe, Dr. C. Dressel, Dr. S. Poppe, Prof. C. Tschierske  
Institute of Chemistry  
Martin Luther University Halle-Wittenberg  
Kurt-Mothes-Str. 2, D-06120 Halle (Saale), Germany  
E-mail: carsten.tschierske@chemie.uni-halle.de

Prof. A. Eremin  
Department of Nonlinear Phenomena  
Institute of Physics  
Otto von Guericke University Magdeburg  
D-39106 Magdeburg, Germany

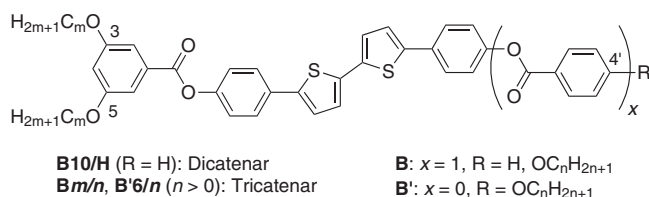
 The ORCID identification number(s) for the author(s) of this article can be found under <https://doi.org/10.1002/adom.202001572>.

© 2020 The Authors. Advanced Optical Materials published by Wiley-VCH GmbH. This is an open access article under the terms of the Creative Commons Attribution-NonCommercial License, which permits use, distribution and reproduction in any medium, provided the original work is properly cited and is not used for commercial purposes.

DOI: 10.1002/adom.202001572

amplification effects, observed in some of the  $Cub_{bi}$  phases,<sup>[27–32]</sup> in the adjacent non-cubic tetragonal<sup>[33]</sup> and the isotropic liquid phases ( $Iso_1^{[3]}$ ) of these achiral polycatenar compounds<sup>[34–36]</sup> has renewed the interest in this class of compounds.<sup>[37–39]</sup> Such spontaneously chiral soft matter systems are of potential technological interest and might also be of importance for the understanding of the mechanism of emergence of uniform chirality.<sup>[40–42]</sup>

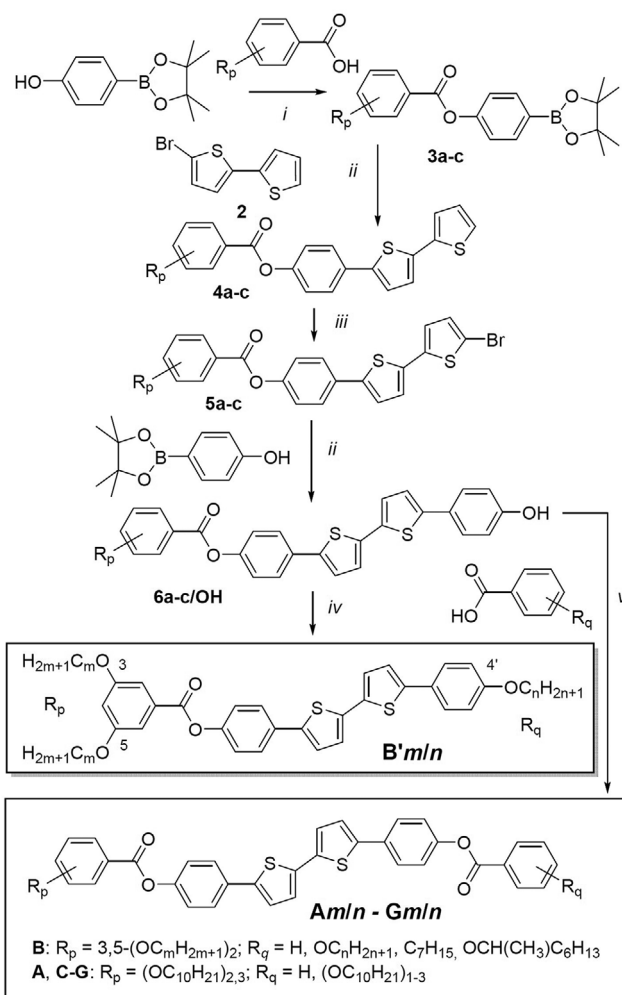
In this work we explore structural modification of 5,5'-diphenyl-2,2'-bithiophene-based polycatenar compounds<sup>[27a,28,29,33,34a]</sup> and we establish the fundamental understanding of these effect on the mesogenic self-assembly at the crossover from lamellar phases to helical networks. The study focuses on new series of compounds with an 3,5-disubstitution pattern at one end and being either non-terminated (**Bm/H**) or terminated with only a single alkyl chain at the other end (**Bm/n** and **B'G/n**). Although the 3,5-disubstitution pattern was used in few cases for the design of columnar LCs,<sup>[43–48]</sup>  $Cub_{bi}$  phases,<sup>[9,24,36,49–52]</sup> and functional liquids,<sup>[53]</sup> it is much less common compared to the huge number of examples of materials with 3,4-disubstitution and the 3,4,5-trisubstitution patterns.<sup>[9]</sup>



It is shown that these new swallow-tailed<sup>[54,55]</sup> compounds provide access to unique materials combining a rich diversity of different modes of self-assembly. Firstly, they offer a new access to the anticlinic-tilted smectic phases ( $SmC_a$ ). Secondly, several higher ordered hexatic ( $Hex$ ) and crystalline lamellar mesophases, including those combining smectic and hexatic self-assembly in a single uniform structure, are observed. Thirdly, chiral and achiral  $Cub_{bi}$  phases, birefringent 3D mesophases and a mirror symmetry broken isotropic liquid ( $Iso_1^{[3]}$ ) involving helically organized bithiophene units are obtained by only tiny changes of the molecular structure. An understanding of this exceptionally wide diversity of self-assembled soft matter structures is based on transitions between tuning fork like and Y-like conformations leading to distinct degrees of intercalation, and thus, to the transition between lamellar organizations and helical self-assembly in networks.

## 2. Methods

The synthesis of the compounds was performed as described in **Scheme 1**, for details see the Supporting Information.<sup>[56]</sup> The compounds were investigated by optical microscopy between crossed or slightly uncrossed polarizers (polarizing microscopy = POM) in films between glass plates and in freely suspended thin films, by differential scanning calorimetry (DSC) and by X-ray scattering, small-angle scattering (SAXS) and wide-angle scattering (WAXS), of powder-like samples and aligned samples. The used instrumentation and other details are described in the Supporting Information.



**Scheme 1.** Synthesis of compounds under investigation. Reagents and conditions: i) DCC, DMAP, DCM, RT; ii)  $[Pd(PPh_3)_4]$ , THF/sat.  $NaHCO_3$ -solution, reflux; iii) NBS, THF, RT, absence of light; iv)  $C_nH_{2n+1}Br$ ,  $K_2CO_3$ ,  $Bu_4NI$ , MEK, reflux; v): 1) benzoic acid +  $SOCl_2$ , 2) **6a-c/OH**, pyridine, DMAP, DCM, RT.

## 3. Results and Discussion

### 3.1. Effects of Alkyl Chain Number and Chain Distribution

For compounds with decyl chains, as example, the effect of the number and position of the chains was investigated (**Figure 1** and Table S6, Supporting Information). As shown in **Figure 1**, there is a transition from a synclinic tilted lamellar phase ( $SmC_s$ ) via  $Cub_{bi}$  to  $Col_{hex}$  upon increasing the number of alkyl chains from three via four to five. Compounds with two chains (e.g., **B10/H**) form only lamellar phases, those with five and more chains exclusively columnar phases ( $Col_{hex}$ , **G10/10**) and those with three and four chains can form lamellar,  $Cub_{bi}$ , as well as columnar phases, depending on structural details. For example, a non-symmetric chain distribution (**A10/10**,<sup>[27a]</sup> **A10/H**,<sup>[27a]</sup> and **B10/10**) is favorable for  $Cub_{bi}$  phase formation, whereas the more symmetric analogs **C10/10** and **D10/10** form only a smectic phase ( $SmC_s$ ).

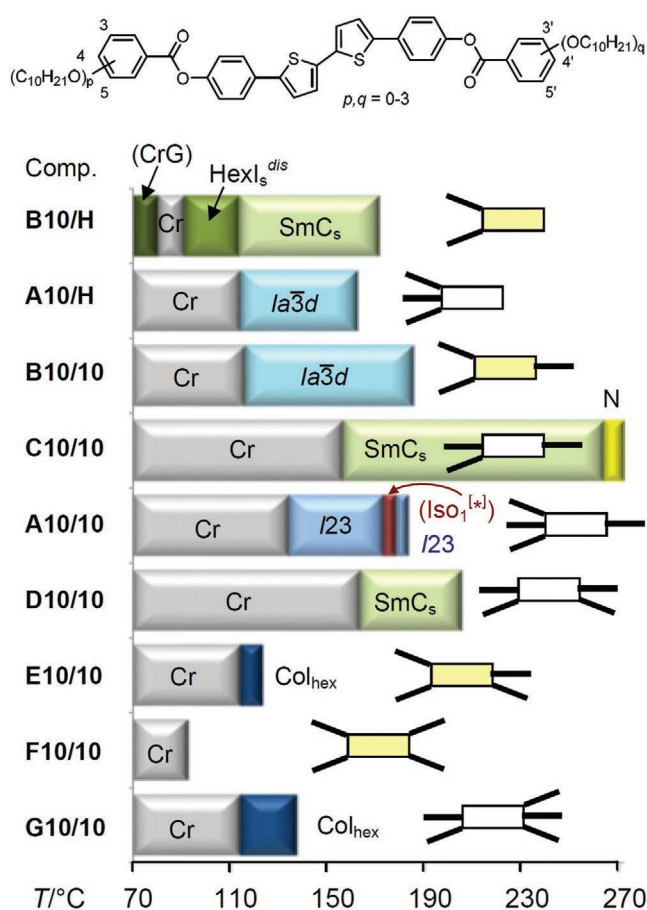


**Figure 1.** Phase transitions of the polycatenar compounds **A–G** as observed on heating and depending on the number and position of the alkyl chains, indicated with pictograms (special focus is on those indicated in yellow); monotropic phases, only observed on cooling, are shown in brackets; Cr, crystalline solid;  $Iso_1^{[*]}$ , mirror symmetry broken isotropic liquid composed of a conglomerate of chiral domains with opposite optical rotation; N, nematic LC phase;  $SmC_s$ , synclinc tilted lamellar LC phase;  $HexI_s^{dis}$ , synclinc tilted hexatic I-phase with  $HexI_s$ -like order of the alkyl chains and  $SmC_s$ -like order of the aromatic cores; CrG, crystalline lamellar G phase;  $Ia\bar{3}d$ , achiral  $Cub_{bi}$  phase with  $Ia\bar{3}d$  space group ( $Cub_{bi}/Ia\bar{3}d$ );  $I23$ ,  $Cub_{bi}$  phase with  $I23$  space group ( $Cub_{bi}^{[sk]}/I23$ ), this cubic phase forms a conglomerate of chiral domains with opposite optical rotation (Figure 7e);  $Col_{hex}$ , hexagonal columnar LC phase; for numerical data on heating and cooling, see Table 1 and Table S6, Supporting Information.

Moreover, the 3,4-disubstitution pattern of the three chain compound **C10/10** favors smectic phases whereas the isomeric compound **B10/10** with 3,5-disubstitution pattern forms a  $Cub_{bi}$  phase, indicating the importance of the molecular shape, being tuning fork like for the smectogenic 3,4-disubstituted compound **C10/10** and Y-like for the cubogenic 3,5-disubstituted compound **B10/10**. Interestingly, the  $Cub_{bi}$  phase is achiral with  $Ia\bar{3}d$  space group for the taper shaped tricatener compounds **A10/H** and **B10/10** which have the alkyl chains at only one end and becomes chiral with  $I23$  space group for the tetracatenars compound **A10/10** with an additional chain at the opposite end. This indicates the importance of chain number (and chain volume) for the selection of the  $Cub_{bi}$  phase type and emergence of mirror symmetry breaking in the soft matter phases

of these achiral molecules. Generally, the 3,5-disubstitution pattern lowers all transition temperatures compared to the related 3,4- and the 3,4,5-substituted compounds, which shifts the LC ranges toward ambient temperature (Figure 1). Only for compound **F10/10** having the 3,5-disubstitution at both ends soft self-assembly is completely lost due to this effect.

### 3.2. Self-Assembly of Compound B10/H with Two Chains at the Same End

Compound **B10/H** has only two chains which are both attached at the same 3,5-substituted end of a rod-like core. It shows three reproducible phase transitions in the DSC traces (Figure 2d and Table 1). On cooling the first transition from the isotropic liquid to a synclinc  $SmC_s$  phase takes place at 169 °C ( $3.0\text{--}2.8\text{ kJ mol}^{-1}$ ). As shown in Figure 2a, the optical extinction brushes in POM are inclined with the direction of the analyzer by an angle of  $\approx 40^\circ$ . This corroborates with a uniform tilt direction of the molecules in adjacent layers (synclinc tilt =  $SmC_s$ ).

The diffuse WAXS with a maximum at  $d = 0.45\text{ nm}$  confirms the liquid-like order in the layers (Figure 2e) and the sharp small angle scattering at  $d = 4.21\text{ to }4.26\text{ nm}$  (Figure 2f, Figure S22c, Supporting Information) corresponds to the molecular length  $L_{mol} = 4.2\text{ nm}$  (Figure 3a). In the 2D scattering patterns of aligned samples the wide angle scattering maximum is inclined to the layer reflection with a tilt angle of  $\beta = 37^\circ$  (Figure 2e and Figure S22a,b, Supporting Information). In a smectic phase with this  $d$ -value and a tilt of  $37^\circ$  the required molecular length would be  $L = d/\cos\beta = 5.3\text{ nm}$ . This is significantly longer than  $L_{mol}$  and therefore excludes the fully intercalated and non-segregated packing shown in Figure 3a. In contrast, the full segregation of the aromatic and aliphatic units in the antiparallel packing with intercalation of only the aromatic cores leads to a layer thickness of  $5.5\text{ nm}$  (Figure 3b) which is close to  $5.3\text{ nm}$ . This mode of packing is not only supported by the segregation of the flexible aliphatic chains from the rigid polyaromatic units, but also allows a side-by-side packing of an equal number of chains and aromatic cores (2/2) in the respective layers, which minimizes the interfacial curvature, and thus supports the lamellar organization.

Upon cooling, at the phase transition at 111 °C, the homeotropic texture becomes smoother and no change is visible in the planar regions, and there is no visible change at the next phase transition at 80 °C, either (Figure 2b,c). The birefringence as well as the inclination of the extinctions in planar alignment is retained in all three phases, meaning that the tilt correlation and the tilt angle do not change markedly (Figure 2a–c). Also the SAXS pattern remains almost the same in all three mesophases, that is, all of them represent synclinc tilted lamellar phases (Figure S22c,e,f, Supporting Information). Clear changes can be observed for the wide-angle scattering, which has a diffuse character in the  $SmC_s$  range and becomes narrower and asymmetric at 111 °C (Figure 2e). The angular scattering profile can be deconvoluted into a sharper peak at  $d = 0.46\text{ nm}$  and a diffuse one with a maximum at  $d = 0.42\text{ nm}$  (Figure 2e, Figure S22g, Supporting Information). This scattering pattern is similar to that reported by Heppke et al. for the so-called  $SmM^*/SmM$  phases of chiral rod-like compounds and their racemates.<sup>[57,58]</sup> Based on the powder X-ray scattering data in

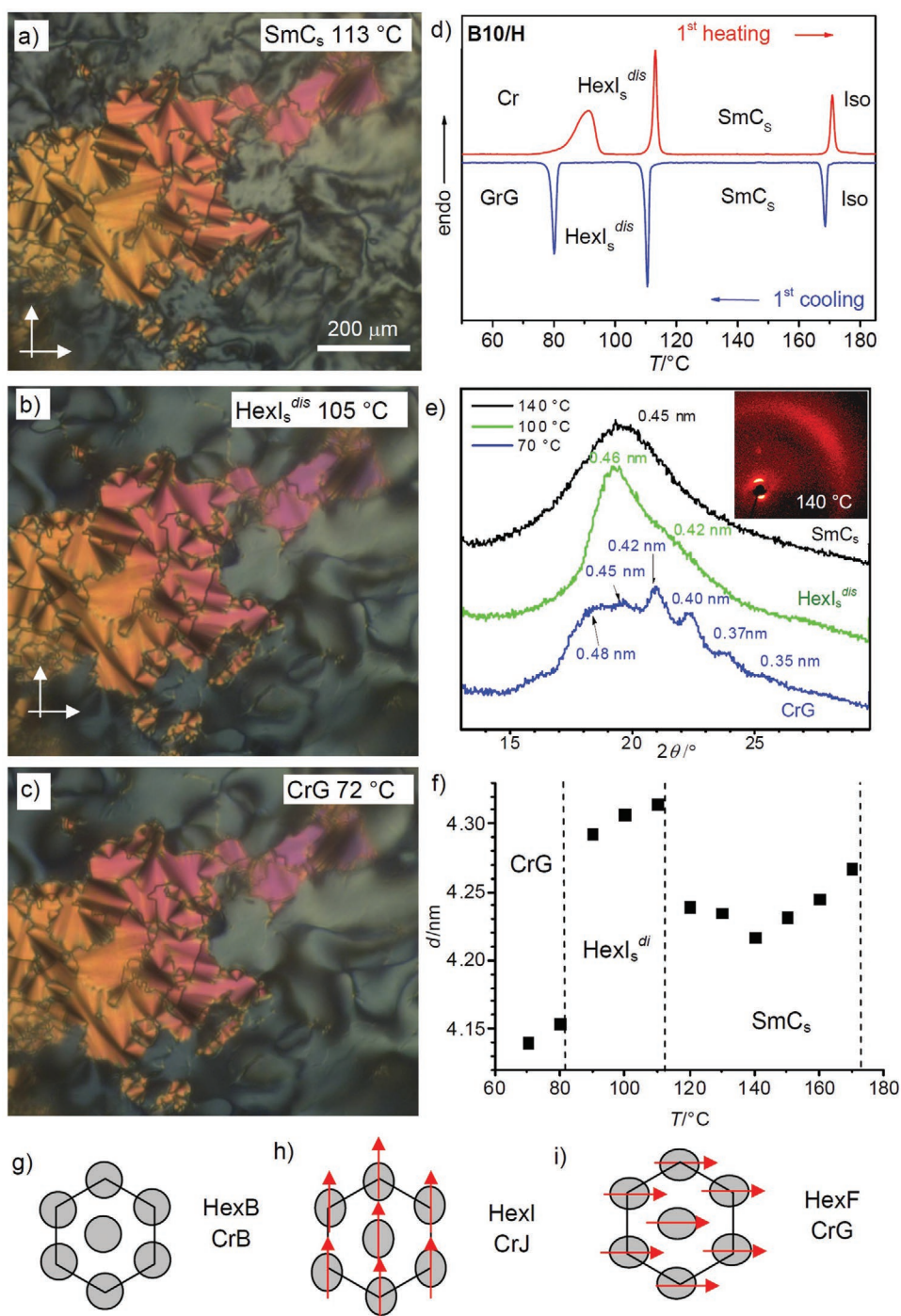
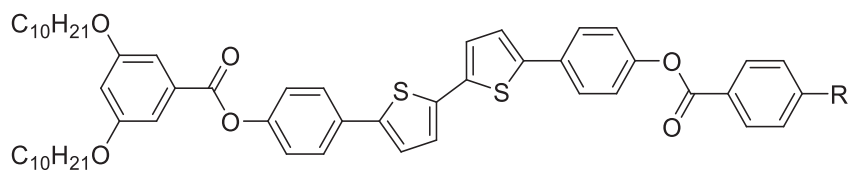


**Figure 2.** Investigation of B10/H. a–c) Textures in the distinct mesophases at the given temperatures as observed between crossed polarizers in planar (red/yellow; view is parallel to the layers) and homeotropic aligned regions (gray; view is along the layer normal); for additional textures, see Figure S8, Supporting Information; d) DSC traces ( $10 \text{ K min}^{-1}$ ); e) WAXS patterns in the distinct mesophases and f) the dependence of the  $d$ -value of the layer reflection on temperature (see also Figure S22, Supporting Information). In g–i), the structures of the hexatic and corresponding crystalline phases are shown schematically; the grey circles and ellipses represent the cross sections of the molecules, the arrows show the tilt direction of the molecules with respect to the 2D lattice, the view is along the layer normal, showing the organization of the molecules in the layers.

Figure 2e,f, we propose a model where aliphatic and aromatic segments are fully segregated (Figure 3b). The synclincic  $\text{SmC}_s$  layers of the aromatic cores, providing the diffuse scattering with a maximum at  $d = 0.42 \text{ nm}$ , alternate with higher ordered

and also synclincic tilted  $\text{HexI}_s$ -like (Figure 2h) alkyl chain layers,<sup>[59–61]</sup> giving rise to the sharper scattering at  $d = 0.46 \text{ nm}$ . Similar segregated structures with different order in the distinct sublayers have been found for swallow-tailed molecules with

**Table 1.** Phase transitions and lattice parameters of the di- and tricatenerans **B10/n** depending on the 4'-alkyl chain length (*n*).



Comp. <sup>a)</sup>	<i>n</i>	Phase transitions <i>T</i> [°C] [ $\Delta H/k$ ] mol <sup>-1</sup> ]	<i>d</i> /nm ( <i>T</i> [°C])	<i>a</i> <sub>cub</sub> /nm ( <i>T</i> [°C])
<b>B10/H</b>	H	H: Cr 91 [10.9] HexI <sub>s</sub> <sup>dis</sup> 113 [5.9] SmC <sub>s</sub> 171 [3.0] Iso C: Iso 169 [-2.8] SmC <sub>s</sub> 111 [-5.9] HexI <sub>s</sub> <sup>dis</sup> 80 [-5.3] CrG <20 Cr	–	4.26 (140) 4.33 (100)
<b>B10/6</b>	OC <sub>6</sub> H <sub>13</sub>	H: Cr 98 [24.9] SmC <sub>s</sub> 151 [0.4] Cub <sub>bi</sub> / <i>la</i> $\bar{3}$ <i>d</i> 191 [1.8] Iso C: Iso 187 [-0.1] Iso <sup>[sk]</sup> 155 [-] Cub <sub>bi</sub> / <i>la</i> $\bar{3}$ <i>d</i> + SmQ + SmC <sub>s</sub> <sup>b)</sup> 76 [-21.7] Cr	4.5 (120)	10.9 (170)
<b>B10/8</b>	OC <sub>8</sub> H <sub>17</sub>	H: Cr 102 [30.5] Cub <sub>bi</sub> / <i>la</i> $\bar{3}$ <i>d</i> 126 [-] M1 138 [-] 189 [2.1] Iso C: Iso 183 [-0.1] Iso <sup>[sk]</sup> 168 [-0.6] Cub <sub>bi</sub> / <i>la</i> $\bar{3}$ <i>d</i> 58 [-19.3] Cr	–	11.0 (180)
<b>B10/10</b>	OC <sub>10</sub> H <sub>21</sub>	H: Cr 116 [53.4] Cub <sub>bi</sub> / <i>la</i> $\bar{3}$ <i>d</i> 185 [2.3] Iso C: Iso 177 [-1.3] Cub <sub>bi</sub> / <i>la</i> $\bar{3}$ <i>d</i> 89 [-33.5] Cr	–	11.3 (150)
<b>B10/16</b>	OC <sub>16</sub> H <sub>33</sub>	H: Cr 114 [74.3] Cub <sub>bi</sub> / <i>la</i> $\bar{3}$ <i>d</i> [-] 160 Cub <sub>bi</sub> <sup>[sk]</sup> /123 173 [2.0] Iso C: Iso 166 [-0.1] Iso <sup>[sk]</sup> 164 [-0.7] Cub <sub>bi</sub> / <i>la</i> $\bar{3}$ <i>d</i> 75 [-17.1] Cr	–	11.5 (130) 17.7 (165)
<b>B10/22</b>	OC <sub>22</sub> H <sub>45</sub>	H: Cr 104 [34.8] Cub <sub>bi</sub> <sup>[sk]</sup> /123 171 [2.8] Iso C: Iso 166 [-1.7] Col <sub>ob</sub> 159 [-0.7] Cub <sub>bi</sub> <sup>[sk]</sup> /123 73 [-43.4] Cr	–	18.1 (140)

<sup>a)</sup>Peak temperatures as obtained by DSC at a scanning rate of 10 K min<sup>-1</sup> on heating (H) or cooling (C); Iso, isotropic liquid; SmQ, low birefringent mesophases with mosaic-like texture, presumably representing a tetragonal 3D phase composed of helical networks with 90° four-way junctions (see Figure 7c),<sup>[33]</sup> M1, low birefringent mesophase with non-specific texture (see Figure S10a, Supporting Information), only observed on heating; Col<sub>ob</sub>, oblique columnar phase (Figures S11 and S21c, Supporting Information); for the other abbreviations, see Figure 1; for DSC traces, see Figure 2a and Figure S2, Supporting Information; for X-ray data, see Tables S1 and S2, Supporting Information; <sup>b)</sup>All three phases can coexist in different ratios depending on the precise conditions; due to slow transitions no DSC peaks can be observed.

perfluorinated alkyl chains<sup>[62]</sup> and could possibly play a role in hexatic phases of LC polymers.<sup>[63]</sup> Due to the combination of the hexatic chain order and SmC<sub>s</sub>-like core order this phase is designated here as HexI<sub>s</sub><sup>dis</sup>. The mesophase at the lowest temperature shows the typical pattern of a tilted crystalline smectic phase, which can satisfactorily be indexed to either G or J (Figure 2e,i and Figure S22h, Supporting Information and Tables S3 and S4, Supporting Information).<sup>[59,60,64]</sup> As the unit cell of the G phase contains a number of molecules closer to the theoretical value of two (Tables S3 and S4, Supporting Information), we prefer this assignment. It appears that this phase results from the simultaneous crystallization of the aromatic and aliphatic layers.

### 3.3. Synclinc Tilted Lamellar Phases of Compounds **B10/n**

The synclinc SmC<sub>s</sub> phase, observed for the two-chain compound **B10/H** is retained for the 4'-hexyloxy substituted tricatener compound **B10/6** where it is stable up to 151 °C; above this temperature it is replaced by an optically isotropic Cub<sub>bi</sub> phase (Table 1). This is in line with the growing interfacial curvature caused by the space required by the additional alkyl chain at the apex, which becomes even more important at higher temperature due to thermal expansion. The layer spacing in the SmC<sub>s</sub> phase is *d* = 4.5 nm which, despite of the expanded molecular length of *L*<sub>mol</sub> = 5.1 nm, is only slightly larger than for **B10/H** without the additional apex-chain. This means that the organization should be dominated by an antiparallel packing of themolecules with fully segregated aromatic and alkyl chain layers, as shown in Figure 3d. This retains the layer spacing of the smectic phase despite of the elongation of the molecule, and is likely to provide an increased tendency

to assume interfacial curvature (2 rods vs 3 chains side-by-side), leading to a transition from lamellar to Cub<sub>bi</sub> phases. The longer homologues show exclusively cubic phases and therefore will be discussed further below.

### 3.4. Anticlinic Smectic Phases of the Swallow-Tailed Compounds **B6/n** with Short 3,5-Chains

In the series of compounds **B6/n** with two shorter hexyloxy chains at the 3,5-substituted end the transition temperatures are much higher and smectic phases can be found up to a longer apex chain length of *n* = 10, for which a Cub<sub>bi</sub> phase coexists with a smectic phase and for the next homologue **B6/12** exclusively the Cub<sub>bi</sub> phase is observed (Table 2). However, as shown below, the smectic phases of all compounds **B6/n** have anticlinic tilt (SmC<sub>a</sub>) and there are no additional hexatic or crystalline low temperature phases, irrespectively if the 4'-chain is odd- or even-numbered (**B6/6** vs **B6/5**, see Table 2), or if it is an alkyl (**B6/6a**) or alkoxy chain.<sup>[65]</sup>

The optical textures of planar samples of the smectic phase show dark extinction brushes parallel to the polarizer and analyzer (Figure 4b,c), thus indicating that the optical axis is parallel to the layer normal. Homeotropic samples show birefringent schlieren textures with dominating two brush disclinations, but also few 4-brush disclinations can be found (Figure 4a). This texture is in line with an anticlinic tilted SmC<sub>a</sub> phase.<sup>[66–70]</sup> In the synclinc tilted SmC<sub>s</sub> phases there would be only 4-brush disclinations, whereas in a non-tilted SmA<sub>b</sub> phase<sup>[71,72]</sup> exclusively two brush disclinations would be expected.<sup>[73]</sup> Thus, the textures in planar as

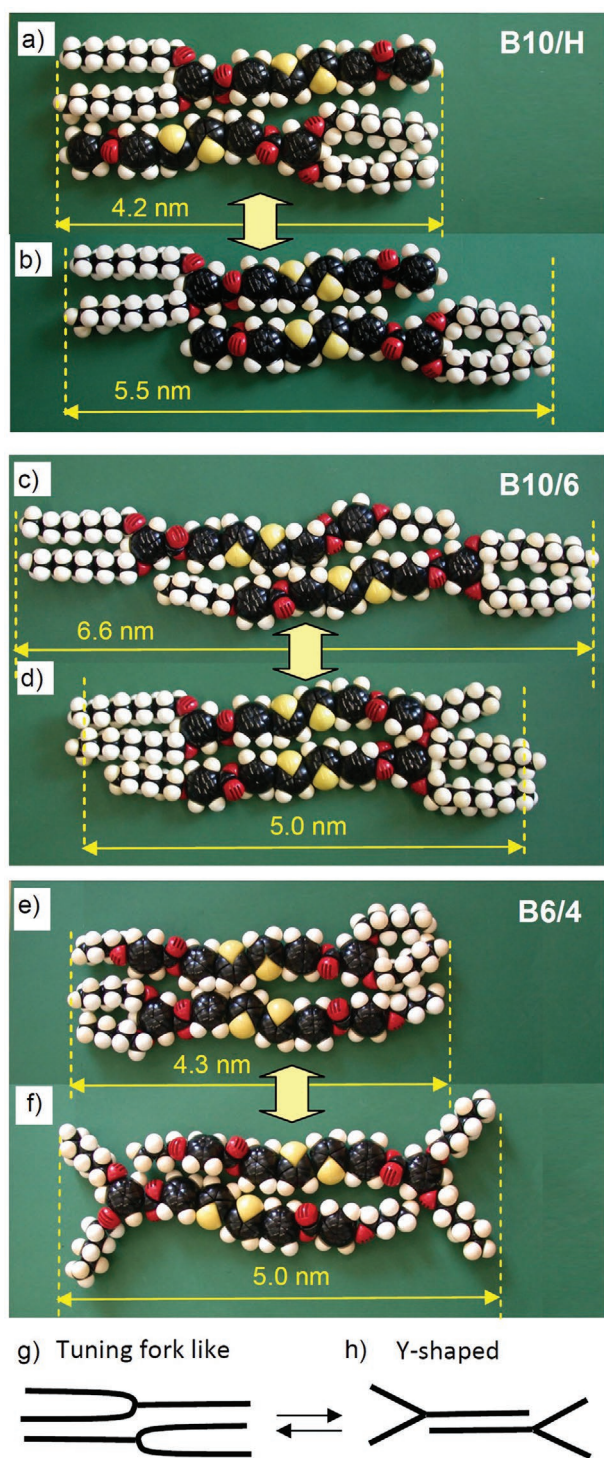


**Figure 3.** Space filling CPK models of pairs of a,b) compound **B10/H** in a) the non-segregated fully intercalated organization ( $L = L_{mol}$ ) and b) segregated organization with intercalation of the aromatic cores only; c,d) compound **B10/6** in c) a non-segregated organization with intercalation of the single 4'-alkyl chains and aromatic cores and d) fully segregated and intercalated pair; e,f) compound **B6/4** in e) shown the fully intercalated organization with a tuning fork like conformation and in f) in a partly intercalated packing with Y-shaped conformations. In (d)  $L$  considers the different ratio of short and long chains. g,h) Schematics of the distinct molecular conformations and their preferred packing modes.

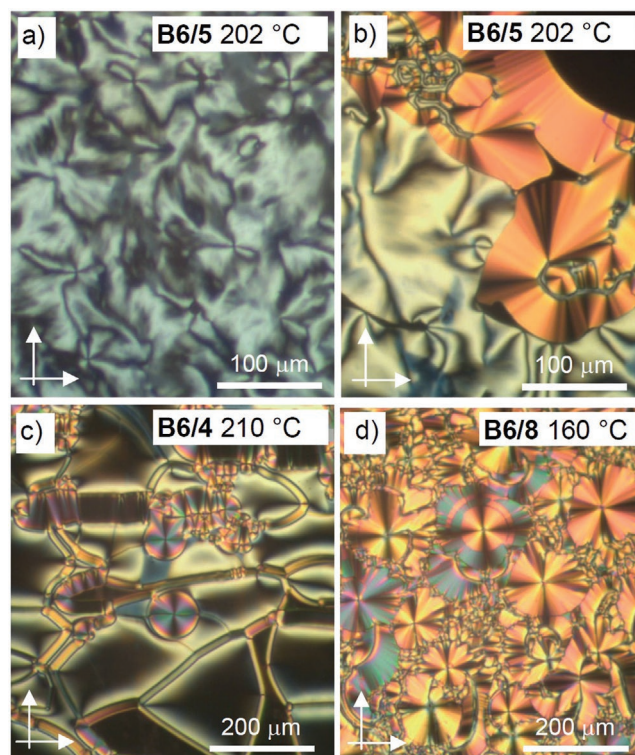


**Figure 4.** a–d) Typical textures of the  $SmC_a$  phases of compounds **B6/n** as observed between crossed polarizers (white arrows) for the indicated compounds at the given temperatures; for additional textures, see Figures S12 and S13, Supporting Information.

well as in homeotropic alignment indicate the formation of an anticlinic  $SmC_a$  phase for the compounds **B6/n** (see also Figure S13, Supporting Information). The anticlinic tilt is corroborated by investigation of freely suspended (FS) films of compound **B6/5** (Figure S16a,b, Supporting Information), where the Schlieren texture, involving half-integer and rare integer defects, remains the same at oblique incidence, independent on the tilt direction of the film with respect to the beam direction.

For compounds **B6/4–B6/10** the layer spacing is around  $d = 4.2$  nm and almost independent on the alkyl chain length (Table 2 and Figure S19a–c, Supporting Information). Only for **B6/10** a slight increase of the layer spacing to  $d = 4.4$  nm is observed. The completely intercalated and fully segregated organization of **B6/4**, shown in Figure 3e, would lead only to a value of  $L = 4.3$  nm for the molecular pairs which would not allow the development of a reasonable tilt and therefore appears less likely. Only mixing of the 4'-alkyl chains with the aromatic rods in the partly intercalated structure in Figure 3f leads to pairs with a length of 5.0 nm allowing a significant tilt. Moreover, in this arrangement the molecules can easily assume a Y-shape, where the 3,5-chains tend to be aligned almost parallel to the layer planes (Figure 3f,h). This reduces the out-of-plane inter-layer fluctuations and favors the anticlinic character of tilt.<sup>[66,74]</sup> Simultaneously, in this Y-conformation the chains are less ordered and therefore no hexatic phase can be observed in the series of compound **B6/n**. This

Y-conformation becomes difficult for longer 3,5-chains (compounds **B10/n**) which favor a parallel alignment of the alkyl chains (Figure 3c) to maximize the dispersion interactions and to minimize the excluded volume.<sup>[75]</sup> The resulting tuning fork like conformation (Figure 3g) supports the synclinal tilt correlation by allowing more interlayer fluctuations.<sup>[74]</sup>

For compounds **6/n** with a longer 4'-alkyl chain ( $n > 10$ ) the intercalation of the incompatible aromatics and alkyl chains becomes unfavorable and these chains are forced to be located in common layers with the 3,5-chains (as shown for **B10/6** and **B6/4** in Figure 3d,e). This enlarges the effective cross-sectional area of the alkyl chains, thus increasing the interface curvature and driving the system from smectic toward  $Cub_{bi}$  phases, as indeed observed upon chain elongation (see Table 2).

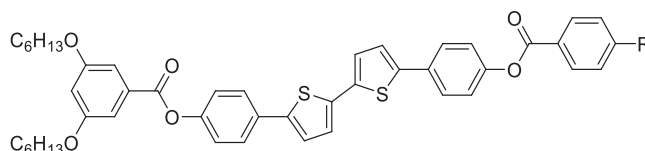
### 3.5. Lamellar Phases in the Series **B'6/n** with Short Cores: Transitions from Anticlinic Smectic to Synclinal Tilted and Non-Tilted Hexatic Phases

The series of compounds **B'6/n** with a shorter five-ring core forms lamellar phases only for the compounds with  $n = 6$  and 8

(Table 3). The X-ray scattering pattern confirms a smectic phase (Figures S23a,b and S24a, Supporting Information) with a diffuse wide angle scattering (Figure 5h) in the high-temperature smectic phase of **B'6/6**. The typical fan-like textures with dark extinctions parallel to the polarizers in planar alignment and a low birefringent schlieren texture with two- and four brush disclinations in homeotropic alignment indicate a  $SmC_a$  phase (Figure 5a,b), which is additionally confirmed by investigation of FS films, as described above for **B6/5** (see Figure S16c, Supporting Information).

The layer spacing of **B'6/6** is with  $d = 4.3$  nm almost the same as for the longer molecule **B6/6** ( $d = 4.2$  nm) and quite a bit longer than the single molecular length of **B'6/6** ( $L_{mol} = 3.9$  nm). This excludes the fully intercalated and completely segregated packing (similar to Figure 3e) and indicates an only partly intercalated packing with the alkyl chain at the apex mixed between the aromatic cores, the same as described for compounds **B6/n** and shown in Figure 3f and Figure S26c, Supporting Information. These pairs have a length  $L = 4.8$  nm allowing a bit smaller tilt of about 20–25°. On cooling **B'6/6** there are additional phase transitions. These transitions are most clearly seen in homeotropic samples, where the schlieren

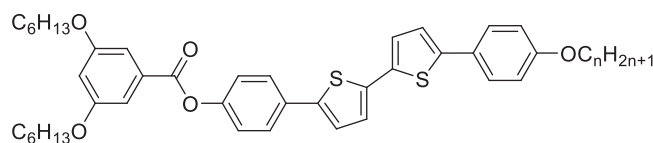
**Table 2.** Phase transitions and lattice parameters of the swallow-tailed tricaténars **B6/n** with different groups at the apex.



Comp. <sup>a)</sup>	R	Phase transitions $T$ [°C] [ $\Delta H$ k] mol <sup>-1</sup>	$d$ /nm ( $T$ [°C])	$a_{cub}$ /nm ( $T$ [°C])
<b>B6/4</b>	OC <sub>4</sub> H <sub>9</sub>	H: Cr 138 [29.0] SmC <sub>a</sub> 215 [1.4] N 220 [0.4] Iso C: Iso 217 [-0.5] N 212 [-1.3] SmC <sub>a</sub> 104 [-21.5] Cr	4.2 (180)	–
<b>B6/5</b>	OC <sub>5</sub> H <sub>11</sub>	H: Cr 139 [32.2] SmC <sub>a</sub> 209 [2.2] Iso C: Iso 207 N 206 [-2.1] <sup>b)</sup> SmC <sub>a</sub> 104 [-25.2] Cr	4.1 (180)	–
<b>B6/6</b>	OC <sub>6</sub> H <sub>13</sub>	H: Cr 123 [25.9] SmC <sub>a</sub> 203 [1.7] Iso <sup>1[sk]</sup> 208 [0.1] Iso C: Iso 205 [-0.1] Iso <sup>1[sk]</sup> 199 [-1.5] SmC <sub>a</sub> 87 [-19.4] Cr	4.1 (160)	–
<b>B6/8</b>	OC <sub>8</sub> H <sub>17</sub>	H: Cr 117 [21.7] SmC <sub>a</sub> 184 [0.9] Iso <sup>1[sk]</sup> 200 [0.1] Iso C: Iso 198 [-0.1] Iso <sup>1[sk]</sup> 177 [-0.8] SmC <sub>a</sub> 96 [-21.7] Cr	4.2 (150)	–
<b>B6/10</b>	OC <sub>10</sub> H <sub>21</sub>	H: Cr 115 [65.3] SmC <sub>a</sub> 145 [-] <sup>c)</sup> M1 150 [-] <sup>c)</sup> M1 + M2 151–156 [-] <sup>c)</sup> Cub <sub>bi</sub> / $la\bar{3}d$ 198 [2.7] Iso C: Iso 191 [-0.3] Iso <sup>1[sk]</sup> 178 [-] <sup>c)</sup> Cub <sub>bi</sub> / $la\bar{3}d$ 105 [-] <sup>c)</sup> SmC <sub>a</sub> 93 [-61.3] Cr	4.4 (120)	10.0 (170)
<b>B6/12</b>	OC <sub>12</sub> H <sub>25</sub>	H: Cr 111 [55.8] Cub <sub>bi</sub> / $la\bar{3}d$ 197 [2.9] Iso C: Iso 189 [-2.1] Cub <sub>bi</sub> / $la\bar{3}d$ 91 [-55.9] Cr	–	10.2 (160)
<b>B6/16</b>	OC <sub>16</sub> H <sub>33</sub>	H: Cr 105 [27.2] Cub <sub>bi</sub> / $la\bar{3}d$ 191 [3.1] Iso C: Iso 182 [-2.1] Cub <sub>bi</sub> / $la\bar{3}d$ 91 [-29.4] Cr	–	10.6 (150)
<b>B6/22</b>	OC <sub>22</sub> H <sub>45</sub>	H: Cr 94 [45.7] Cub <sub>bi</sub> / $la\bar{3}d$ 180 [2.4] Iso C: Iso 173 [-2.1] Cub <sub>bi</sub> / $la\bar{3}d$ 78 [-44.6] Cr	–	11.3 (140)
<b>B6/6a</b>	C <sub>6</sub> H <sub>13</sub>	H: Cr 124 [28.9] SmC <sub>a</sub> 206 [2.0] Iso <sup>1[sk]</sup> 209 [0.2] Iso C: Iso 206 [-0.1] Iso <sup>1[sk]</sup> 203 [-1.9] SmC <sub>a</sub> 88 [-23.3] Cr	4.2 (150)	–
<b>B6/7Me</b>	OCH(CH <sub>3</sub> )C <sub>6</sub> H <sub>13</sub>	H: Cr 116 [32.0] Cub <sub>bi</sub> / $la\bar{3}d$ 130 [1.8] Iso C: Iso 121 [-1.5] Cub <sub>bi</sub> / $la\bar{3}d$ < 20 Cr	–	8.9 (125)

<sup>a)</sup>Peak temperatures as obtained by DSC at a scanning rate of 10 K min<sup>-1</sup> on heating (H) or cooling (C); SmC<sub>a</sub>, anticlinic tilted SmC phase; M2, 3D mesophases with medium birefringence (see Figure 7i); for the other abbreviations, see Figure 1 and Table 1; for DSC traces, see Figure S3a–h, Supporting Information; for X-ray data, see Tables S1 and S5, Supporting Information; <sup>b)</sup>Enthalpy for both transitions Iso-N-SmC<sub>a</sub>; <sup>c)</sup>Enthalpy value cannot be determined because the transition is slow; these transition temperatures were obtained by optical investigations.

**Table 3.** Phase transitions and lattice parameters of the swallow-tailed tricaténars **B'6/n** depending on the length of the 4'-alkyl chain (*n*).



Comp. <sup>a)</sup>	<i>n</i>	Phase transitions <i>T</i> [°C] [ $\Delta H$ kJ mol <sup>-1</sup> ]	<i>a</i> <sub>cub</sub> /nm ( <i>T</i> [°C])
<b>B'6/6</b>	6	H: M 109 [4.3] HexI <sub>s</sub> <sup>dis</sup> 144 [7.3] HexF <sub>s</sub> 147 [0.1] SmC <sub>a</sub> 159 [4.4] Iso C: Iso 156 [-4.3] SmC <sub>a</sub> 145 [-0.1] HexF <sub>s</sub> 141 [-6.5] HexI <sub>s</sub> <sup>dis</sup> 104 [-3.3] M	–
<b>B'6/8</b>	8	H: Cr 114 [10.9] HexB 125 HexF <sub>s</sub> 128 [2.9] <sup>b)</sup> SmC <sub>a</sub> 135 [1.0] Iso <sub>1</sub> <sup>[sk]</sup> 142 [0.2] Iso C: Iso 140 [-0.3] Iso <sub>1</sub> <sup>[sk]</sup> 130 [-1.0] SmC <sub>a</sub> 127 HexF <sub>s</sub> 123 [-2.7] <sup>b)</sup> HexB 107 [-11.2] Cr	–
<b>B'6/10</b>	10	H: Cr 113 [44.8] SmQ + Cub <sub>bi</sub> / <i>la</i> $\bar{3}d$ <sup>c)</sup> 128 [0.2] Iso <sub>1</sub> <sup>[sk]</sup> 137 [2.2] Iso C: Iso 131 [-0.2] Iso <sub>1</sub> <sup>[sk]</sup> 118 [-] SmQ + Cub <sub>bi</sub> / <i>la</i> $\bar{3}d$ <sup>c)</sup> 103 [-26.1] Cr	9.2(115)
<b>B'6/12</b>	12	H: Cr 114 [52.3] Cub <sub>bi</sub> / <i>la</i> $\bar{3}d$ 133 [2.8] Iso C: Iso 123 [-1.1] Cub <sub>bi</sub> / <i>la</i> $\bar{3}d$ 98 [-51.1] Cr	9.4 (125)
<b>B'6/16</b>	16	H: Cr 102 [62.3] Cub <sub>bi</sub> / <i>la</i> $\bar{3}d$ 128 [3.6] Iso C: Iso 125 [-3.0] Cub <sub>bi</sub> / <i>la</i> $\bar{3}d$ 92 [-52.6] Cr	9.6(120)
<b>B'6/20</b>	20	H: Cr 106 [90.9] Cub <sub>bi</sub> / <i>la</i> $\bar{3}d$ 124 [3.9] Iso C: Iso 119 [-3.2] Cub <sub>bi</sub> / <i>la</i> $\bar{3}d$ 88 [-85.2] Cr	10.0 (115)

<sup>a)</sup>Peak temperatures as obtained by DSC at a scanning rate of 10 K min<sup>-1</sup> on heating (H) or cooling (C); HexB, hexatic B phase (molecules are orthogonal to the layer planes); M, unknown low temperature lamellar phase (see Figures S15 and S24b, Supporting Information); for other abbreviations, see Figure 1 and Table 1; for DSC traces, see Figure S4, Supporting Information; for X-ray data, see Tables S1 and S5, Supporting Information; <sup>b)</sup>Transition enthalpy for both transitions CrB-HexF<sub>s</sub>-SmC<sub>a</sub>; <sup>c)</sup>Both phases coexist in different ratio depending on the conditions.

texture becomes mosaic like at the first phase transition at 145 °C (Figure 5d) and further changes with reduction of birefringence at the next transition at 141 °C (Figure 5f). In the planar sample the first transition at 145 °C is associated with a decrease of birefringence and the dark brushes of the fans become birefringent, indicating the onset of a synclitic tilt (Figure 5c). No significant change can be observed at the next phase transition at 141 °C (Figure 5e).

In the SAXS patterns of **B'6/6** the layer reflection is retained and the *d*-value increases on cooling (Figure 5i) mainly attributed to the alkyl chain stretching in the more ordered lamellar phases.<sup>[76]</sup> Moreover, there is a pronounced change of the shape of the WAXS (Figure 5h). The diffuse wide angle scattering in the SmC<sub>a</sub> phase narrows slightly at 145 °C and then splits into two scatterings with very different width at the next transition at 141 °C. Based on the optical textures and the shape of the WAXS we attribute the first transition at 145 °C to a transition to a HexF<sub>s</sub> phase (Figures 5h and 2h).<sup>[77]</sup> The shape of the powder WAXS pattern in the next low temperature phase is characterized by a relative sharp scattering at *d* = 0.46 nm which we attribute to HexI<sub>s</sub>-like packing in the layers of the alkyl chains (Figure 2i) and an additional diffuse scattering due to the SmC<sub>s</sub>-like ordered aromatic cores, similar as observed for the HexI<sub>s</sub><sup>dis</sup> phase of compound **B10/H**.

An additional transition at 104 °C obviously leads to a soft crystalline lamellar phase which is not further specified (M, see Figures S15 and S24, Supporting Information). It appears that reduction of the aromatic core length increases the influence of alkyl chain packing on LC self-assembly, and thus a similar sequence of smectic, hexatic and crystalline lamellar phases, as also found for **B10/H** with longer chains, but reduced chain number, can be observed.

A sequence of different lamellar phases is also observed for the next homologue **B'6/8** (Figure 6), however the phases are distinct from those of **B'6/6**. The high temperature phase is again a SmC<sub>a</sub> phase (Figure 6a). On cooling the birefringence of the schlieren texture decreases, the fans become broken (Figure 6b) and the wide-angle scattering sharpens slightly, in line with a SmC<sub>a</sub>-HexF<sub>s</sub> transition (Figure 6e). Again the layer spacing increases due to the chain stretching (Figure 6f), but this effect is even larger than for **B'6/6**. In powder patterns the wide angle scattering remains symmetric and in aligned samples it has a maximum around the equator, as typical for the HexF phase (Figure 6e and Figure S25, Supporting Information).<sup>[59,60,78]</sup> The stripe patterns across the fans, occurring at the transition to HexF (Figure 6b) indicates the transition to a synclitic tilt (HexF<sub>s</sub>). Finally the homeotropic areas become optically isotropic, the *d*-value of the layer scattering reaches *d* = 5.0 nm indicating a non-tilted organization. This *d*-value is much larger than *L*<sub>mol</sub> = 4.2 nm (Figure 6f), but close to the length of pairs of molecules with non-segregated partly intercalated organization (similar to Figure 3c, *L* = 5.1 nm, see Figure S27b, Supporting Information). All these observations confirm a transition from the anticlinic SmC<sub>a</sub> phase, at first assuming a synclitic tilt upon growing packing density in the HexF<sub>s</sub> phase to a non-tilted organization of the molecules in the HexB phase (Figure 2g). As typical for the transition to hexatic phases, the orientational order parameter (*S*) determined from the  $\chi$ -scan of the WAXS of aligned samples,<sup>[79]</sup> increases significantly at the transition to the hexatic phases (Figure 6e, right inset and Figure S25, Supporting Information). FS film investigations indicate a layer-by-layer SmC<sub>a</sub>-HexF<sub>s</sub> transition and a following continuous decreasing birefringence indicates



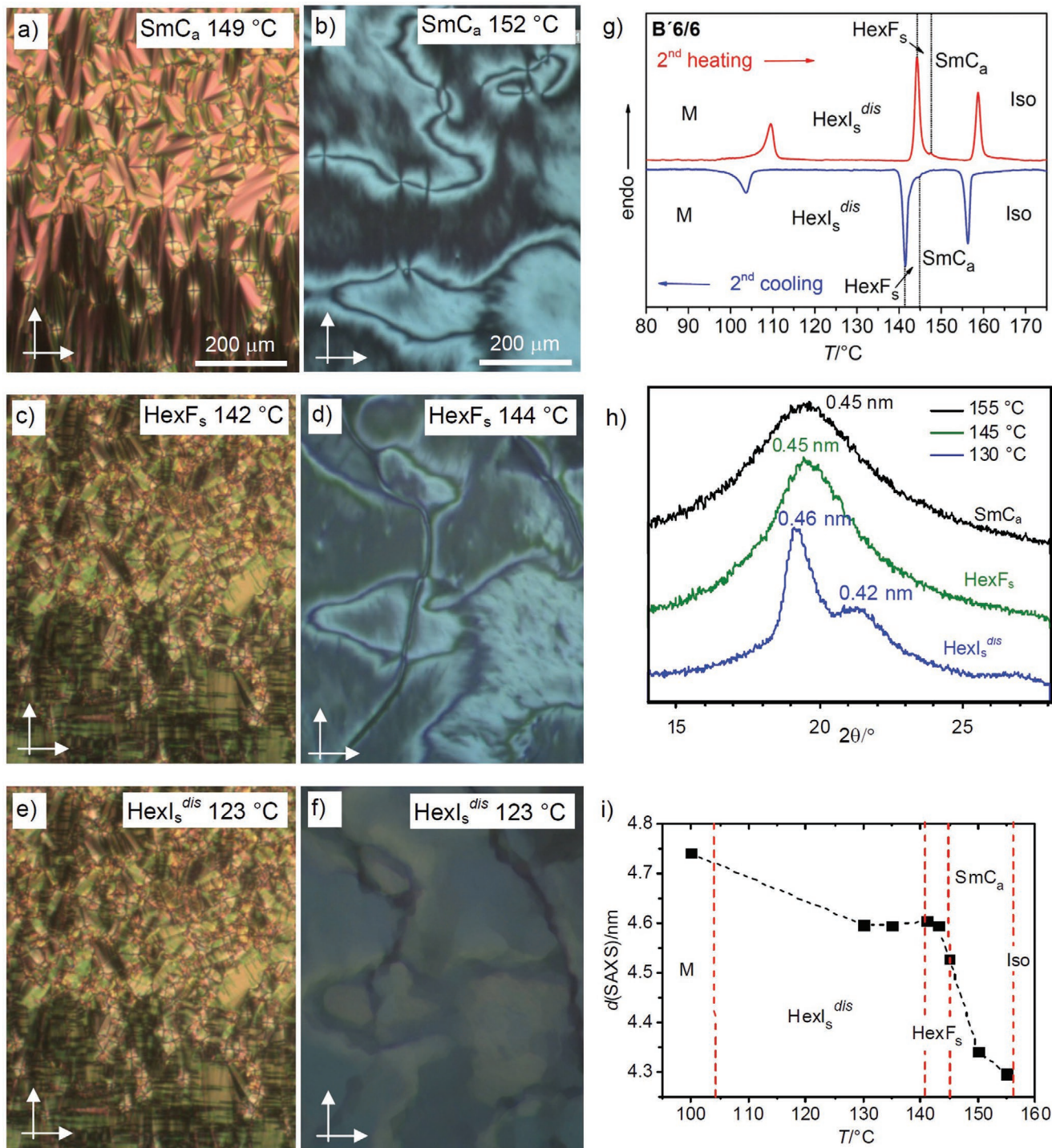


**Figure 5.** Investigation of compound B'6/6. a–f) Optical textures in planar (left) and homeotropic samples (right) as observed between crossed polarizers (white arrows) on cooling at the given temperatures in the indicated phases (for the transition Hexl<sub>s</sub><sup>dis</sup>-M, see Figure S15, Supporting Information); g) DSC heating and cooling traces at 10 K min<sup>-1</sup>; h) shape of the WAXS with *d*-values of the maxima and i) plots of the *d*-values of layer spacing depending on temperature; for more details, see Figures S23 and S24, Supporting Information).

a continuous reduction and removal of the tilt at the transition to HexB (Figure S16c–f, Supporting Information). For the following homologues of the series B'6/*n* the smectic and hexatic phases are removed and replaced by the Cub<sub>bi</sub> phase.

### 3.6. Cub<sub>bi</sub> Phases

The formation of the optically isotropic Cub<sub>bi</sub> phases from the birefringent SmC phases (SmC<sub>s</sub>/SmC<sub>a</sub>) is indicated by the

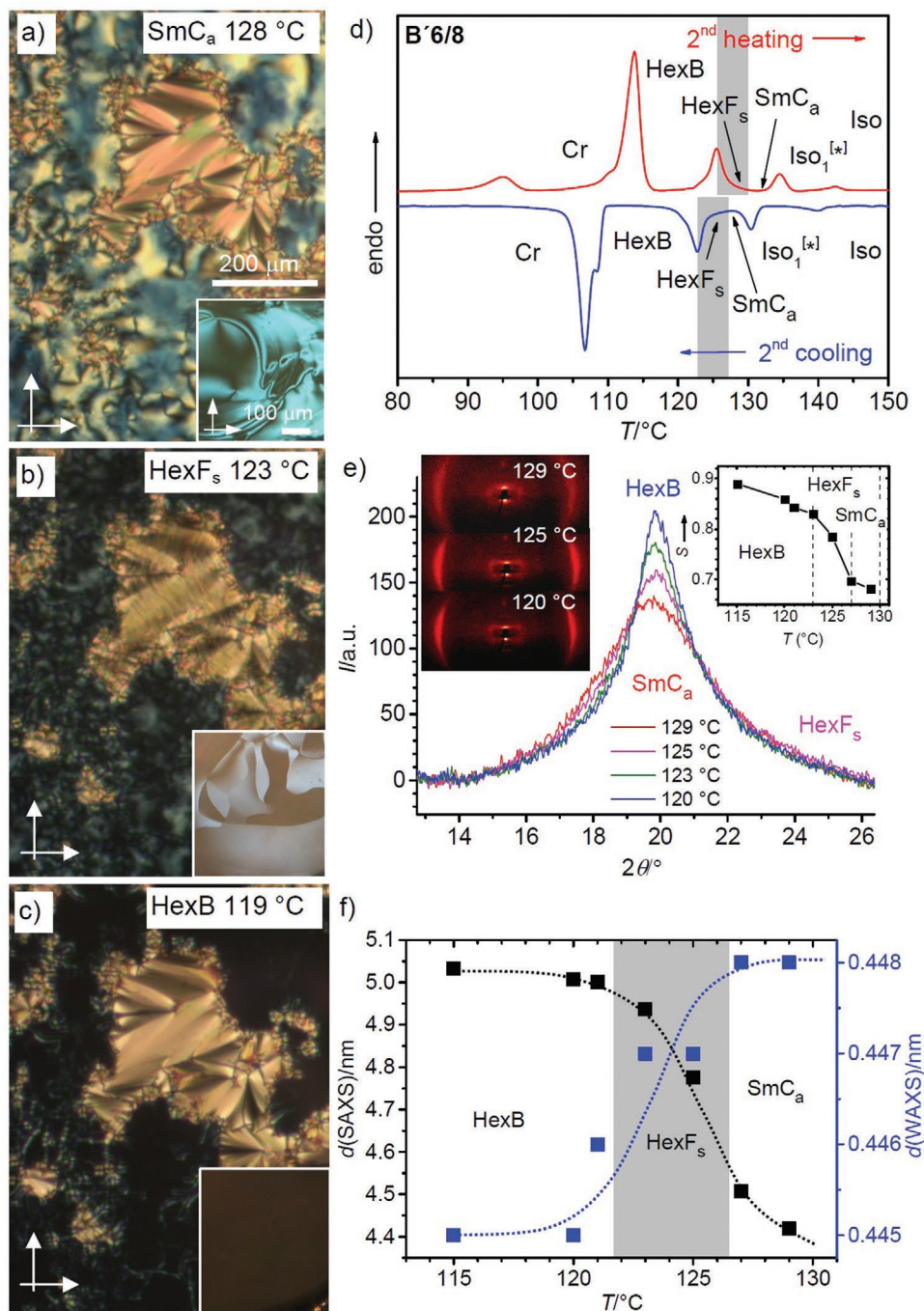


**Figure 6.** Investigation of the lamellar phases of compound **B'6/8**. a–c) Optical textures as observed between crossed polarizers in samples combining regions with planar alignment (fan-textures) with those having homeotropic alignment (gray), on cooling at the given temperatures in the indicated phases; the insets show the corresponding textures of freely suspended films (for details, see Figure S16c–f, Supporting Information); d) DSC heating and cooling traces at  $10 \text{ K min}^{-1}$ ; e) change of the shape of the WAXS (see also Figure S25, Supporting Information), and f) plots of the  $d$ -values of layer spacing and WAXS maximum depending on temperature; in e) the inset on the left shows the 2D scattering pattern of an aligned sample at the indicated temperature and that on the right shows the development of the orientational order parameter ( $S$ ) depending on temperature (see Figure S25, Supporting Information).

appearance of optically isotropic areas (Figure 7g), whereas the transition from the isotropic liquids (Iso, Iso<sub>1</sub><sup>[\*]</sup>) to Cub<sub>bi</sub> is only detected by a significant increase of viscosity. While the liquids flow under gravity, the isotropic Cub<sub>bi</sub> phases represent

viscoelastic solids which occasionally can grow as single crystals.<sup>[80]</sup> In most cases this transition is associated with a small DSC peak, often accompanied by a significant hysteresis of the phase transition on cooling. Moreover, transitions involving

Cub<sub>bi</sub> phases are often slow and then become invisible in the DSC traces. In the X-ray scattering patterns the cubic phases are identified by the presence of several sharp small angle Bragg peaks together with a completely diffuse wide angle scattering, the latter confirming the LC state (Figures S20b and S21b, Supporting Information). The cubic lattice type can be deduced from the relative positions of the most intense small angle scatterings either corresponding to the (211) and (220) indices of the  $Ia\bar{3}d$  lattice (Figure 7a and Figure S20a, Supporting Information) or the (321), (400) and (420) indices of the  $I23$  lattice (Figure 7b and Figure S21a, Supporting Information).<sup>[15,27a,28–31]</sup> The assignment to the distinct lattices is for polycatenar compounds easily confirmed by optical investigations between not fully crossed polarizers, where the  $I23$  phase shows a conglomerate of dark and bright domains which invert their brightness by rotating the analyzer into the opposite direction (Figure 7e).<sup>[27a,28]</sup> This indicates the presence of chiral domains as typical for the triple network  $I23$  structure (Figure 7b).<sup>[27a]</sup> In contrast, for the Cub<sub>bi</sub> phases with double network structure and space group  $Ia\bar{3}d$  (Figure 7a) no such domains can be found (Figure 7f).<sup>[27a,29,81]</sup> In the Cub<sub>bi</sub> phases the rod-like cores are organized in the networks which are separated by the continuum of the alkyl chains (Figure 7a,b). The orientation of the rods is on average perpendicular or slightly tilted to the networks and in this configuration the crowded periphery of the polycatenars inhibits a parallel arrangement of the tightly packed polyaromatic rods. This mismatch leads to a helical twist  $\Phi$  along the networks (Figure 7d)<sup>[27,28,34]</sup> and the network junctions allow a transmission of uniform helix sense over macroscopic distances. The double gyroid with  $Ia\bar{3}d$  space group (Figure 7a)<sup>[14,15,19,82]</sup> involves two interwoven enantiomorphic networks with opposite helicity and connected by three way junctions, leading to an achiral overall structure. This helically twisted organization in the achiral  $Ia\bar{3}d$  phases of rod-like molecules was recently supported by soft resonant X-ray scattering.<sup>[83]</sup> In this structure the twist between two three-fold junctions is 70.5°, which must fit with the total of the twists  $\Phi$  between adjacent molecules located on the way between two junctions.<sup>[27]</sup> If a mismatch arises other alternative structures are formed. The most common is the triple network structure with  $I23$  symmetry (Figure 7b),<sup>[39]</sup> previously known as “ $Im\bar{3}m$ ” phase,<sup>[24,26]</sup> which is chiral, not only because the chirality of the three networks cannot compensate, but also as a result of preferred homochiral helix packing.<sup>[27]</sup> The Cub<sub>bi</sub>/ $Ia\bar{3}d$  phase was found in all three series of compounds **Bm/n** and **B'6/n** after crossing a certain critical length of the 4'-alkyloxychain of  $n \geq 8$  for the series **B10/n** and  $n \geq 10$  for the series **B6/n** and **B'6/n**. The Cub<sub>bi</sub>/ $I23$  phase requires long chains at both ends (**B10/n** with  $n \geq 16$ ).

As obvious from the comparison of compounds **B6/8** and **B6/7Me** with the same number of carbon atoms, but with linear and branched apex chains, respectively, chain branching favors Cub<sub>bi</sub> phase formation over lamellar self-assembly, due to the larger effective cross section of these conformationally more disordered branched chains (Table 2). Increasing alkyl chain dynamics (by increasing temperature or by chain branching) does not only change the interface curvature and shifts the aggregate shape and phase type from lamellar to Cub<sub>bi</sub>, it also distorts the core-core interactions and thus decreases the phase

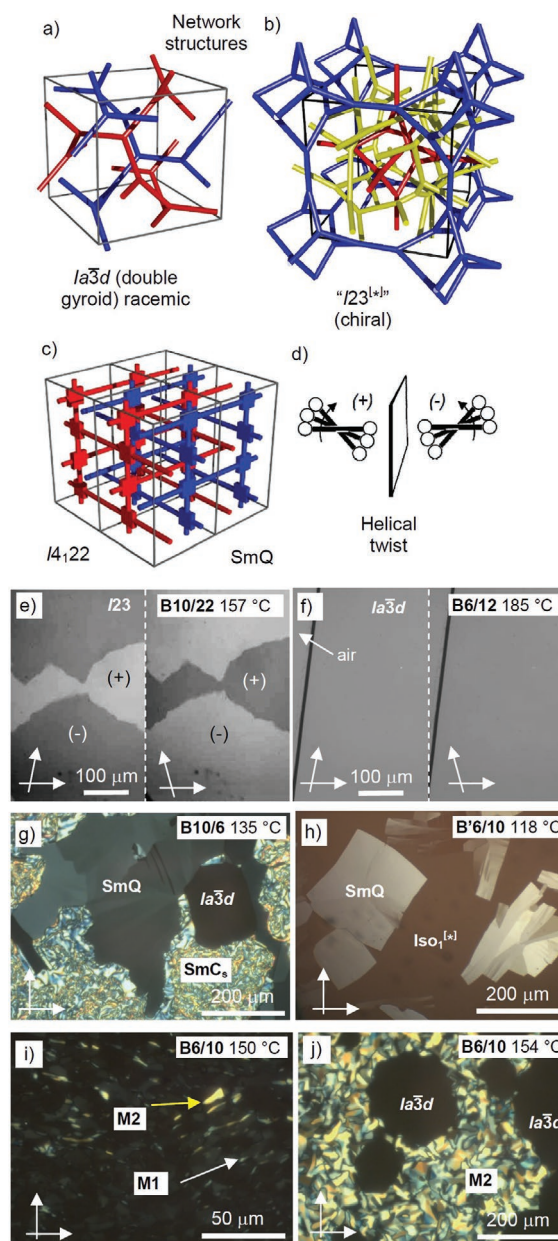


**Figure 7.** a–c) The major helical network structures presently known for polycatenar mesogens;<sup>[33,39]</sup> d) development of the helical twist by clashing of the end groups attached to rod-like cores;<sup>[32b]</sup> the helices propagate along the red, blue, and yellow networks. e,f) Textures of Cub<sub>bi</sub> phases observed under slightly uncrossed polarizers (in e) the contrast is enhanced). g–j) Representative optical textures of birefringent intermediate phases as observed between crossed polarizers; g) coexisting SmC<sub>s</sub>, Cub<sub>bi</sub>/ $Ia\bar{3}d$ , and SmQ phases on cooling **B10/6** from Iso<sub>1</sub><sup>[32]</sup> between non-treated microscopic glass plates (for textures in an ITO cell, see Figure S9, Supporting Information); h) SmQ phase of **B'6/10** as growing from Iso<sub>1</sub><sup>[32]</sup> on slow cooling (for the SmQ-Cub<sub>bi</sub>/ $Ia\bar{3}d$  transition, see Figure S10b, Supporting Information) and i,j) development of the M1 and M2 phases on heating compound **B6/10**, i) low birefringent mosaic texture (white arrow) of the M1 phase (see also Figure S10a, Supporting Information) with bright crystallites of the M2 phase with higher birefringence (yellow arrow) which in j) become dominating and transform into the Cub<sub>bi</sub>/ $Ia\bar{3}d$  phase on further heating. b) Reproduced with permission.<sup>[39]</sup> Copyright 2020, The Royal Chemical Society. c) Reproduced with permission.<sup>[33]</sup> Copyright 2020, Wiley-VCH.

transition temperatures, including the Iso<sub>1</sub><sup>[\*]</sup>-Iso transition, that is, the upper critical temperature of mirror symmetry breaking. Therefore, the transition temperatures of **B6/7Me** are much lower and the Iso<sub>1</sub><sup>[\*]</sup> phase of **B6/8** is suppressed (see also Section 3.8).

The cubic phases in the series **B6/n** and **B'6/n** have exclusively the *Ia3d* space group, whereas in the series of compounds **B10/n** with longer 3,5-chains an additional cubic phase with *I23* space group is observed for  $n \geq 16$ . For **B10/16** the formation of either the chiral Cub<sub>bi</sub><sup>[\*]</sup>/*I23* or the achiral Cub<sub>bi</sub>/*Ia3d* phase depends on the conditions; on heating there is a *Ia3d* – *I23* transition whereas on cooling only the *Ia3d* phase is found (Table 1). For **B10/22** with the longest alkyl chain exclusively the *I23* phase is observed on heating and cooling. This shows that a certain minimum chain length (or chain volume) is required for the formation of the mirror symmetry broken Cub<sub>bi</sub><sup>[\*]</sup>/*I23* phase.<sup>[15b,27–32]</sup> Only in one case, for the compound with the longest total chain length (**B10/22**), a columnar phase (Col<sub>ob</sub>) accompanies the Cub<sub>bi</sub><sup>[\*]</sup>/*I23* phase as a high temperature phase, resulting from the further increased interface curvature provided by this long chain (see Table 1 and Figure S11, Supporting Information). However, the Col<sub>ob</sub> phase is metastable and can only be observed on cooling, whereas on heating a direct Cub<sub>bi</sub><sup>[\*]</sup>/*I23*-Iso transition takes place.

### 3.7. Birefringent Mesophases with 3D Lattice

For compounds with a total chain length of  $m + n = 16$  to 18, being located at the transition from lamellar to Cub<sub>bi</sub>/*Ia3d* organization (compounds **B10/6**, **B10/8**, **B6/10**, and **B'6/10**, see Tables 1–3) Cub<sub>bi</sub> phase formation is accompanied by the formation of other birefringent mesophases with 3D lattice, either representing distorted versions of the Cub<sub>bi</sub>/*Ia3d* phase,<sup>[20]</sup> or arising from alternative helix packings (e.g., SmQ, see Figure 7c<sup>[33]</sup>). The formation of these intermediate phases at the lamellae-to-network transition is strongly dependent on the conditions, including thermal history of the sample, heating and cooling rates, boundary conditions, and modes of alignment. Often their formation is slow and therefore these transitions do not show up in the DSC traces (see Figures S2–S4, Supporting Information). Usually they are metastable and are rapidly replaced by the developing Cub<sub>bi</sub>/*Ia3d* phase, being the more stable phase. Therefore, their investigation, especially by X-ray scattering, is difficult and we can only describe qualitatively some typical observations. One of the intermediate phases is likely to be the SmQ phase which is characterized by a low birefringent mosaic-like texture, typically appearing gray, even in thick samples.<sup>[34]</sup> It is often observed on cooling from the mirror symmetry broken Iso<sub>1</sub><sup>[\*]</sup> phase (see next section) and once formed it rapidly transforms into the Cub<sub>bi</sub>/*Ia3d* phase on further cooling or isothermal with time. This helical network phase with tetragonal *I4<sub>1</sub>22* symmetry and 90° four-way network junctions was recently solved (Figure 7c).<sup>[33]</sup> It is proposed to represent an intermediate state at the transition from the mirror symmetry broken Iso<sub>1</sub><sup>[\*]</sup> phase with uniform helix sense to the racemic *Ia3d* phase, requiring the inversion of the helix sense for half of the networks. We assume that the low birefringent phases occurring at the Iso<sub>1</sub><sup>[\*]</sup>-Cub<sub>bi</sub> transition of

**B10/6** (Figure 7g) and **B'6/10** (Figure 7h) are likely to represent a SmQ phase, too. Also the low birefringent phase designated as M1 (compounds **B10/8**, **B6/10**, Tables 1 and 2) could possibly be the SmQ phase, though a specific texture cannot be observed in these cases (Figure 7i and Figure S10a, Supporting Information) and confirmation by X-ray scattering is not possible due to metastability and coexistence with other phases. Only the M2 phase of **B6/10**, having higher birefringence (Figure 7j), is likely to be different and related to similar birefringent 3D phases with tetragonal,<sup>[11,24,84–87]</sup> orthorhombic<sup>[88]</sup> or rhombohedral symmetry.<sup>[89]</sup>

In summary, formation of birefringent 3D phases is a general phenomenon, associated with the lamellar-Cub<sub>bi</sub>/*Ia3d* cross-over. In each of the investigated series it is observed for only one or two homologues with a certain chain length of  $m + n = 16$  to 18. Upon further chain elongation the non-cubic phases are removed and exclusively the Cub<sub>bi</sub> phases remain with the sequence *Ia3d* → *I23*. Notably, in the investigated series of compounds there are obviously no birefringent 3D phases occurring as intermediate phases at the transition between the *Ia3d* and *I23* phases.

### 3.8. Mirror Symmetry Broken Isotropic Liquid Phase Iso<sub>1</sub><sup>[\*]</sup>

The formation of an isotropic liquid mesophase showing a conglomerate of chiral domains with opposite optical rotation (Iso<sub>1</sub><sup>[\*]</sup>, see Figure 8a,b) is associated with the lamellar-to-Cub<sub>bi</sub> transition upon alkyl chain elongation, too. This chiral liquid formed by achiral molecules is considered as a percolated liquid with a dynamic helical network structure, which provides a long range transmission of uniform chirality in the enantiomeric domains of the conglomerate, but without assuming a long range cubic lattice.<sup>[29,30–32,34a]</sup> The helical self-assembly is supported by transiently chiral helical molecular conformations, as provided by the twisted 5,5'-diphenyl-2,2'-bithiophene core of the reported compounds.<sup>[32,34a]</sup>

Interestingly, FS films can be drawn in the Iso<sub>1</sub><sup>[\*]</sup> range; Figure 8d shows the FS film of the Iso<sub>1</sub><sup>[\*]</sup> phase of **B'6/8**. Those films have non-uniform thickness (Figure S28e, Supporting Information) and appear without any visible texture between crossed polarizers, though the films are metastable and limited in size. Like liquid fibers subjected to the Rayleigh-plateau instability, liquid films exhibit thinning instability and collapse too.<sup>[90]</sup> In smectics, it is the 1D periodic structure which is responsible for stabilization of freely suspended films.<sup>[91]</sup> The unexpected film formation of the Iso<sub>1</sub><sup>[\*]</sup> phase can be attributed to the dynamic network structure,<sup>[30]</sup> which, like in the case of polymers (and some oligomesogens<sup>[92]</sup>), stabilizes the films and leads to a non-Newtonian behavior. Additionally, correlation of the nano clusters can be induced by the free surfaces, similar to some nematic phases forming dynamic metastable films.<sup>[93]</sup> The films are even stable across the Iso<sub>1</sub><sup>[\*]</sup>-Iso transition. Also heating of the FS SmC<sub>a</sub> film to the SmC<sub>a</sub>-Iso<sub>1</sub><sup>[\*]</sup> transition temperature leads to Iso<sub>1</sub><sup>[\*]</sup> films (Figure 8e,f and Figure S27, Supporting Information). Only in sufficiently thick films (>100 μm) mirror symmetry breaking takes place and domains of opposite chirality can be observed, thinner films appear to be achiral. Interestingly, these chiral domains have

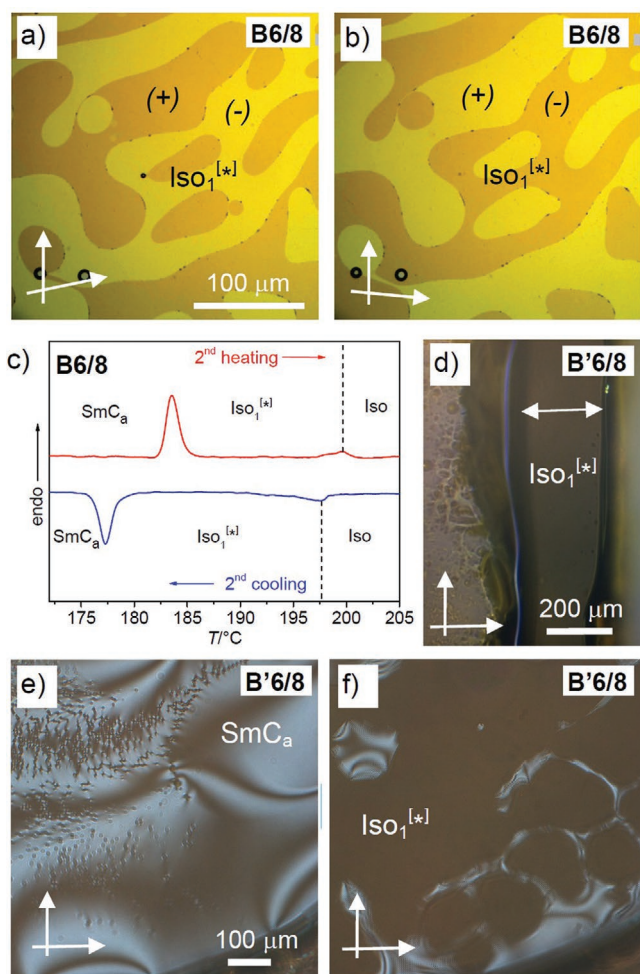


**Figure 8.** a,b) Chiral conglomerate of the mirror symmetry broken  $\text{Iso}_1^{[*]}$  phase of **B6/8** at 185 °C as observed in  $\approx 50 \mu\text{m}$  thick films between two glass plates and between polarizers, being slightly uncrossed in different directions; c) DSC traces showing the  $\text{SmC}_a$ - $\text{Iso}_1^{[*}$ ]- $\text{Iso}$  transitions on heating and cooling ( $10 \text{ K min}^{-1}$ ). d–f) FS films of **B'6/8** as observed between crossed polarizers (white arrows); d) FS films drawn in the  $\text{Iso}_1^{[*]}$  phase between two supports (right and left) at  $T = 138 \text{ °C}$ ; the film thickness is 200–800 nm; e,f)  $\text{SmC}_a$ - $\text{Iso}_1^{[*}$  transition as observed on slow heating of a FS film drawn in the  $\text{SmC}_a$  phase (see also Figure S28, Supporting Information). A film without polarizers is shown in Figure S28e, Supporting Information; FS films between twisted polarizers show chiral domains only if the film has sufficient thickness and then the chiral domains rapidly fuse with formation of a homochiral film which also appears uniform.

an unequal distribution with one sign of chirality dominating. Once this imbalance has developed the film becomes rapidly homochiral, due to the huge chirality amplification capability of the  $\text{Iso}_1^{[*]}$  phase. The capability of chirality amplification was previously reported for samples between glass substrates as shown in Figure S4, Supporting Information of ref. [34a]. Due to the ubiquitous presence of tiny chirality sources in the environment, in most cases the FS  $\text{Iso}_1^{[*]}$  films of sufficient thickness appear homogeneously chiral almost from the beginning.

In the series of compounds **Bm/n** and **B'6/n** the formation of the  $\text{Iso}_1^{[*]}$  phase is associated with the  $\text{SmC}$ -to- $\text{Cub}_{\text{bi}}/Ia\bar{3}d$  transition, irrespectively if the  $\text{SmC}$  phase is synclinal or

anticlinal. It is observed for a medium chain length around  $n = 6$ –10 (**B10/n**:  $n = 6, 8$ , **B6/n**:  $n = 6$ –10 and **B'6/n**:  $n = 8, 10$ , see Tables 1–3). For most compounds it is only observed on cooling as a monotropic phase replacing the  $Ia\bar{3}d$  phase, but for compounds **B'6/8**, **B6/8** and **B6/6a** it is an enantiotropic phase occurring directly above  $\text{SmC}_a$  (without accompanying  $\text{Cub}_{\text{bi}}$  phase) and having the broadest enantiotropic  $\text{Iso}_1^{[*]}$  range for **B6/8**. As shown in Figure 8c, the  $\text{Iso}$ - $\text{Iso}_1^{[*}$  transition is associated with a small enthalpy in the DSC traces which is attributed to the chirality synchronization.<sup>[30,31]</sup> Previous temperature dependent SAXS experiments have indicated a continuously decreasing line width, and hence, growing correlation length of the helical aggregates around the continuous  $\text{Iso}$ - $\text{Iso}_1^{[*}$  transition, and a jump to resolution limited Bragg peaks at the discontinuous  $\text{Iso}_1^{[*}$  to  $\text{Cub}_{\text{bi}}$  transition.<sup>[31,34a]</sup> The  $\text{Iso}$ - $\text{Iso}_1^{[*}$  transition was also investigated by optical rotation and circular dichroism.<sup>[27a]</sup> Based on all these investigations the model of a dynamic network structure of the  $\text{Iso}_1^{[*}$  phase was suggested.<sup>[30–32,34a,42]</sup> Recent results of NMR relaxation and NMR diffusion measurements at the  $\text{Cub}_{\text{bi}}$ - $\text{Iso}$ - $\text{Iso}$  transitions of other achiral polycatenar molecules support this model of a local  $\text{Cub}_{\text{bi}}$ -like structure of the  $\text{Iso}_1$  type phases.<sup>[94a]</sup> and theoretical work supports the importance of network formation for mirror symmetry breaking.<sup>[95]</sup> In the case reported here, the spontaneous chirality evolves by the chirality synchronization in the dynamic helical superstructure of the  $\text{Iso}_1^{[*}$  phase.<sup>[32]</sup> In fact, there is some similarity with the  $\text{Iso}_1^*$  phase occurring besides chirality frustrated LC phases of permanently chiral molecules (\*),<sup>[11a,b,96,97]</sup> the most prominent example being the BPIII phase.<sup>[98]</sup> It should be noted, that  $\text{Iso}$ - $\text{Iso}_1$  transitions have previously been reported to occur besides cubic LC phases,<sup>[15b,97a]</sup> but the helical network structure and the capability of these  $\text{Iso}_1$  phases of mirror symmetry breaking, first reported in ref. [27a], were not recognized at that time. Moreover, liquid state polymorphism is a general feature of complex liquids, which is not yet fully recognized,<sup>[42,99,100]</sup> but of great importance for biosystems, too.<sup>[32,101]</sup>

The  $\text{Iso}_1^{[*}$  phase and related isotropic mesophases often appear in proximity to the  $\text{SmQ}$  phase, a birefringent 3D phase with tetragonal lattice (Figure 7c)<sup>[33,96]</sup> and therefore, it is likely that the local structure in the dynamic networks of the  $\text{Iso}_1^{[*}$  phases of the investigated compounds is similar to the helical network structure with  $90^\circ$  four-way junctions as recently proposed for this  $\text{SmQ}$  phase ( $\text{Iso}_1^{[*}$  ( $\text{SmQ}$ )).<sup>[33]</sup> For compounds **B6/6**, **B6/8**, **B'6/8** and **B6/6a** the  $\text{Iso}_1^{[*}$  phase appears between the achiral isotropic liquid ( $\text{Iso}$ ) and the anticlinal  $\text{SmC}_a$  phase, in these cases without any competing  $\text{SmQ}$  or  $Ia\bar{3}d$  phase and it is formed on heating as well as on cooling, without the strong hysteresis being typical for the  $\text{Iso}_1^{[*}$   $\rightarrow$   $Ia\bar{3}d$  transition (Figure 8c). In these cases the  $\text{SmQ}$ -like local network structure in the  $\text{Iso}_1^{[*}$  phase transforms directly into an achiral lamellar phase, without requiring a helix inversion. Interestingly, as soon as the  $Ia\bar{3}d$  phase emerges in the phase sequence, also other 3D phases ( $\text{SmQ}$ ,  $\text{M1}$ ,  $\text{M2}$ ) appear, which can be explained by the required helix inversion at the  $\text{Iso}_1^{[*}$ - $Ia\bar{3}d$  transition. The transition from the conglomerate of the chiral  $\text{Iso}_1^{[*}$  phases to the racemic  $Ia\bar{3}d$  phase requires a helix inversion for half of the networks which is a collective process in the networks and therefore requires a significant activation energy which

makes this inversion slow.<sup>[33]</sup> Therefore, a homogeneous chiral intermediate phase, not requiring helix inversion (e.g., SmQ) is formed first. However, it is metastable and in a second step slowly transforms into the racemic  $Ia\bar{3}d$  phase by partial helix inversion. As the achiral  $Ia\bar{3}d$  phase becomes dominating with growing chain length, the chiral Iso<sub>1</sub><sup>[\*]</sup> phase disappears together with the SmQ phase and the other non-cubic 3D phases. It is likely that with chain elongation the local structure of the Iso/Iso<sub>1</sub> phase becomes  $Ia\bar{3}d$  like, which is achiral.<sup>[102]</sup>

Whereas for the compounds **Bm/n** and **B'6/n** exclusively the chiral Iso<sub>1</sub><sup>[\*]</sup><sub>(SmQ)</sub> and achiral isotropic liquid phases could be observed, in the related series of the tetracatenars compounds **Am/n** with one more chain and significantly larger chain volume (3,4,5-trisubstitution, see compound **A10/10** in Figure 1) the Iso<sub>1</sub><sup>[\*]</sup> phase appears again and occurs in proximity to the mirror symmetry broken Cub<sub>bi</sub><sup>[\*]</sup>/I23 phase.<sup>[27a,29,34]</sup> Therefore, it appears likely that there are two different types of Iso<sub>1</sub><sup>[\*]</sup> phases having different local network structures, being either SmQ-like with 90° four-way junctions (Figure 7c) for those located close to the lamellar–Cub<sub>bi</sub>/Ia $\bar{3}d$  cross-over (Iso<sub>1</sub><sup>[\*]</sup><sub>(SmQ)</sub>), compounds **B** and **B'** and I23-like with almost 120° three-way junctions for those occurring besides the Cub<sub>bi</sub><sup>[\*]</sup>/I23 phase (Iso<sub>1</sub><sup>[\*]</sup><sub>(I23)</sub>; compounds **A**, see Figure 7b). An achiral Iso<sub>1</sub> phase, presumably with local  $Ia\bar{3}d$  structure was detected for related 3,5-substituted tricaténars with azobenzene cores<sup>[52,103]</sup> and 3,4,5-substituted benzil based tetracatenars<sup>[30,31]</sup> which completes the overall sequence Iso<sub>1</sub><sup>[\*]</sup><sub>(SmQ)</sub>–Iso<sub>1</sub><sub>(Ia $\bar{3}d$ )</sub>–Iso<sub>1</sub><sup>[\*]</sup><sub>(I23)</sub> of the percolated network liquids upon alkyl chain expansion (see Figure 9). This series of percolated liquids is analogous to the sequence SmQ–Cub<sub>bi</sub>/Ia $\bar{3}d$ –Cub<sub>bi</sub><sup>[\*]</sup>/I23 observed for the related LC phases with long range periodic network structure. In contrast to the Iso<sub>1</sub><sup>[\*]</sup> to Ia $\bar{3}d$  transformation, which is accompanied by birefringent 3D phases, no such intermediate phases could be found for the Iso<sub>1</sub><sup>[\*]</sup> to I23 transition,<sup>[29–31]</sup> probably because no helix inversion is required for the transition between these two chiral phases.

#### 4. Summary

This work provides a systematic investigation of the structure-property relations of a new kind of swallow-tailed polycatenar compounds at the transition from lamellar to helical network phases. The compounds involve the functional 5,5'-diphenyl-2,2'-bithiophene core, which is of interest as fluorescent (AIE active) and charge carrying unit for the development of new multifunctional organic electronic materials. As well known, the local organization of these  $\pi$ -conjugated rods determines the application relevant properties and, therefore, the understanding of the fundamental rules of their soft self-assembly is of general interest.

The effect of the alkyl chain number and alkyl chain distribution is shown in Figure 1. The main focus is on swallow-tailed compounds having the rarely used 3,5-disubstitution pattern at one end combined with a non-substituted or 4'-alkyloxysubstituted apex (Scheme 1). Their conformation can change depending on alkyl chain length and temperature between a Y-like and a tuning fork like shape (Figure 3g,h); the main self-assembled structures formed by these compounds and their development depending on the molecular structure are summarized

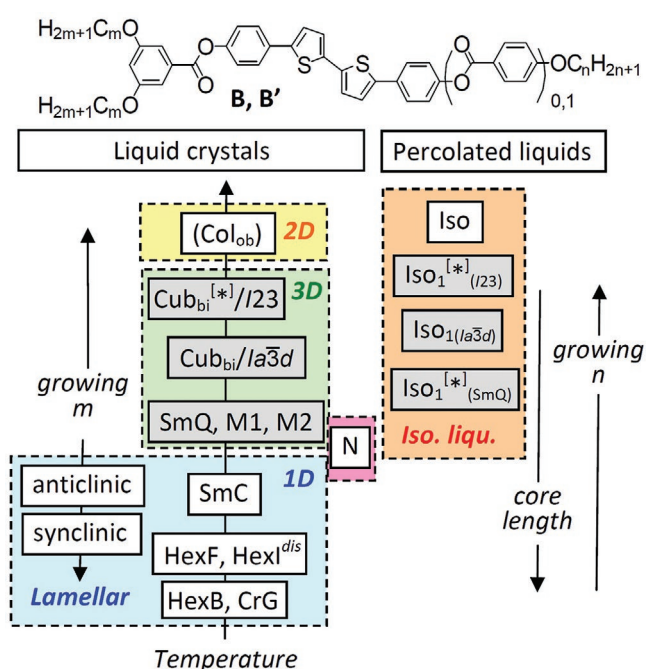


**Figure 9.** Overview over the structure-mesophases relations of the investigated compounds; Iso<sub>1</sub><sub>(Ia $\bar{3}d$ )</sub> and Iso<sub>1</sub><sup>[\*]</sup><sub>(I23)</sub> were not observed for compounds **B** and **B'**, but were added for completeness of the phase sequences; gray background indicates helical network phases.

in Figure 9. By chain elongation a transition from lamellar phases to bicontinuous cubic phases, first with achiral  $Ia\bar{3}d$  space group and upon further chain elongation with the chiral and spontaneous mirror symmetry broken Cub<sub>bi</sub><sup>[\*]</sup>/I23 phase (Figure 7a,b), followed by a columnar phase (Col<sub>ob</sub>), is observed.

The lamellar phases represent tilted smectic phases which are synclinic tilted if the 3,5-chains are sufficiently long, and become anticlinic tilted for shorter chains. Thus, this molecular structure provides a new class of anticlinic SmC<sub>a</sub> materials, being of interest for antiferroelectric and orthoconic LCs for display applications.<sup>[67]</sup> Another specific feature of these compounds is the formation of a series of hexatic low temperature phases. At the transition to the hexatic phases the tilt correlation becomes synclinic (HexF<sub>s</sub>, HexI<sub>s</sub><sup>dis</sup>) or the tilt is removed (HexB, see Figure 2g–i). In addition, new variants of hexatic phases combining hexatic order of the alkyl chains with more disordered aromatic cores (HexI<sub>s</sub><sup>dis</sup>) were observed.

Finally, it is shown that the SmC–Cub<sub>bi</sub>/Ia $\bar{3}d$  transitions are accompanied by the formation of additional modes of self-assembly, among them birefringent 3D mesophases, as the tetragonal SmQ phase (Figure 7c) and a mirror symmetry broken isotropic liquid phase (Iso<sub>1</sub><sup>[\*]</sup>, Figure 8). It is shown that for the latter freely suspended films can be drawn, which can become local mirror symmetry broken and even homogeneously chiral, due to the chirality synchronization in the dynamic helical network with proposed SmQ-like local structure. A sequence of chiral (Iso<sub>1</sub><sup>[\*]</sup>) and achiral (Iso<sub>1</sub>) percolated liquids with local network structures, resembling those of the adjacent cubic and non-cubic LC network phases is proposed to occur depending on the alkyl chain length and thus changing intermolecular twist (Figure 9).

Overall, this work contributes to the general understanding of the soft matter self-assembly at the lamellae-network transition and the mechanism of spontaneous mirror symmetry breaking in fluids, being of technological interest for the development of novel functional materials and devices.

## Supporting Information

Supporting Information is available from the Wiley Online Library or from the author.

## Acknowledgements

This work was supported by the Deutsche Forschungsgemeinschaft (Ts 39/24-2 and ER 467/8-2).

Open access funding enabled and organized by Projekt DEAL.

## Conflict of Interest

The authors declare no conflict of interest.

## Keywords

antclinic smectic phases, bicontinuous cubic phases, bithiophenes, helical networks, hexatic phases, liquid crystals, mirror symmetry breaking, polycatenars

Received: September 13, 2020

Revised: October 23, 2020

Published online: November 25, 2020

- [1] Y.-X. Hu, W.-J. Li, P.-P. Jia, X.-Q. Wang, L. Xu, H.-B. Yang, *Adv. Opt. Mater.* **2020**, *8*, 2000265.
- [2] Y. Tsutsui, W. Zhang, S. Ghosh, T. Sakurai, H. Yoshida, M. Ozaki, T. Akutagawa, S. Seki, *Adv. Opt. Mater.* **2020**, *8*, 1902158.
- [3] T. Yasuda, H. Ooi, J. Morita, Y. Akama, K. Minoura, M. Funahashi, T. Shimomura, T. Kato, *Adv. Funct. Mater.* **2009**, *19*, 411.
- [4] a) J. Mei, N. L. C. Leung, R. T. K. Kwok, J. W. Y. Lam, B. Z. Tang, *Chem. Rev.* **2015**, *115*, 11718. b) Y. Li, S. Liu, T. Han, H. Zhang, C. Chuah, R. T. K. Kwok, J. W. Y. Lam, B. Z. Tang, *Mater. Chem. Front.* **2019**, *3*, 2207; c) H.-T. Feng, J. W. Y. Lam, B. Z. Tang, *Coord. Chem. Rev.* **2020**, *406*, 213142.
- [5] F. Song, Z. Zhao, Z. Liu, J. W. Y. Lam, B. Z. Tang, *J. Mater. Chem. C* **2020**, *8*, 3284.
- [6] L. Wang, Q. Li, *Adv. Funct. Mater.* **2016**, *26*, 10.
- [7] W. Goodby, P. J. Collings, T. Kato, C. Tschierske, H. Gleeson, P. Raynes, *Handbook of Liquid Crystals*, 2nd ed., Wiley-VCH, Weinheim, Germany **2014**.
- [8] Q. Li, *Nanoscience with Liquid Crystals. – From Self-Organized Nanostructures to Applications*, Springer, Cham, Switzerland **2014**.
- [9] a) J. Malthete, H. T. Nguyen, C. Destrade, *Liq. Cryst.* **1993**, *13*, 171; b) H. T. Nguyen, C. Destrade, J. Malthete, *Adv. Mater.* **1997**, *9*, 375; c) M. Gharbia, A. Gharbi, H. T. Nguyen, J. Malthete, *Curr. Opin. Colloid Interf. Sci.* **2002**, *7*, 312; d) D. W. Bruce, *Acc. Chem. Res.* **2000**, *33*, 831; e) H. T. Nguyen, C. Destrade, J. Malthete, in *Handbook of Liquid Crystals* (Eds: D. Demus, J. Goodby, G. W. Gray, H.-W. Spiess, V. Vill), Wiley-VCH, Weinheim, Germany **1998**, pp. 865–900; f) W. Weissflog, in *Handbook of Liquid Crystals*, 2nd ed. (Eds: J. W. Goodby, J. P. Collings, T. Kato, C. Tschierske, H. F. Gleeson, P. Raynes), Wiley-VCH, Weinheim, Germany **2014**, pp. 89–174.
- [10] a) J. Malthete, A. M. Levelut, N. H. Tinh, *J. Phys. Lett.* **1985**, *46*, 875; b) N. H. Tinh, J. Malthete, C. Destrade, *Mol. Cryst. Liq. Cryst. Lett.* **1985**, *2*, 133; c) N. H. Tinh, C. Destrade, A. M. Levelut, J. Malthete, *J. Phys.* **1986**, *47*, 553; d) D. Guillon, A. Skoulios, J. Malthete, *Europhys. Lett.* **1987**, *3*, 67; e) C. Destrade, N. H. Tinh, A. Roubineau, A. M. Levelut, *Mol. Cryst. Liq. Cryst.* **1988**, *159*, 163; f) A. M. Levelut, J. Malthete, C. Destrade, N. H. Tinh, *Liq. Cryst.* **1987**, *2*, 877; g) N. T. Nguyen, C. Destrade, J. Malthete, *Liq. Cryst.* **1990**, *8*, 797.
- [11] a) I. Nishiyama, *Chem. Rec.* **2009**, *9*, 340; b) M. Yoneya, *Chem. Rec.* **2011**, *11*, 66; c) E. Nishikawa, J. Yamamoto, H. Yokoyama, *J. Mater. Chem.* **2003**, *13*, 1887; d) E. Nishikawa, E. T. Samulski, *Liq. Cryst.* **2000**, *27*, 1463; e) A. Yoshizawa, *Polym. J.* **2012**, *44*, 490.
- [12] a) C. Tschierske, *J. Mater. Chem.* **2001**, *11*, 2647; b) C. Tschierske, *Annu. Rep. Prog. Chem. Sect. C* **2001**, *97*, 191; c) C. Tschierske, *Isr. J. Chem.* **2012**, *52*, 935; d) C. Tschierske, in *Handbook of Liquid Crystals*, 2nd ed., Vol. 5 (Eds: J. W. Goodby, J. P. Collings, T. Kato, C. Tschierske, H. F. Gleeson, P. Raynes), Wiley-VCH, Weinheim, Germany **2014**, pp. 1–88.
- [13] C. Tschierske, *Angew. Chem., Int. Ed.* **2013**, *52*, 8828.
- [14] L. Han, S. Che, *Adv. Mater.* **2018**, *30*, 1705708.
- [15] a) G. Ungar, F. Liu, X. B. Zeng, in *Handbook of Liquid Crystals* (Eds: W. Goodby, P. J. Collings, T. Kato, C. Tschierske, H. Gleeson, P. Raynes), Wiley-VCH, Weinheim, Germany **2014**; b) S. Kutsumizu, *Isr. J. Chem.* **2012**, *52*, 844.
- [16] T. Kato, J. Uchida, T. Ichikawa, T. Sakamoto, *Angew. Chem., Int. Ed.* **2018**, *57*, 4355.
- [17] M. Maldovan, A. M. Urbas, N. Yufa, W. C. Carter, E. L. Thomas, *Phys. Rev. B* **2002**, *65*, 165123.
- [18] M. L. Lynch, P. T. Spicer, *Bicontinuous Liquid Crystals*, CRC Press, Taylor & Francis Group, Boca Raton, FL **2005**.
- [19] a) J. M. Seddon, R. H. Templer, in *Handbook of Biological Physics* (Eds: R. Lipowsky, E. Sackmann), Elsevier Science B.V., Amsterdam **1995**, pp. 97–160; b) S. T. Hyde, in *Handbook of Applied Surface and Colloid Chemistry* (Ed: K. Holmberg), Wiley-VCH, Weinheim, Germany **2001**, pp. 299–332; c) L. van 't Hag, S. L. Gras, C. E. Conn, C. J. Drummond, *Chem. Soc. Rev.* **2017**, *46*, 2705.
- [20] a) A. J. Meuler, M. A. Hillmyer, F. S. Bates, *Macromolecules* **2009**, *42*, 7221; b) E. L. Thomas, *Sci. Chin. Chem.* **2018**, *61*, 25.
- [21] S. Hyde, S. Andersson, K. Larsson, Z. Blum, T. Landh, S. Lidin, B. W. Ninham, *The Language of Shape: The Role of Curvature in Condensed Matter: Physics, Chemistry and Biology*, Elsevier Science B.V., Amsterdam **1997**.
- [22] A. H. Schoen, *NASA Technical Note TN D-5541* **1970**.
- [23] a) X. Zeng, S. Poppe, A. Lehmann, M. Prehm, C. Chen, F. Liu, H. Lu, G. Ungar, C. Tschierske, *Angew. Chem., Int. Ed.* **2019**, *58*, 7375; b) S. Poppe, X. H. Cheng, C. L. Chen, X. B. Zeng, R. B. Zhang, F. Liu, G. Ungar, C. Tschierske, *J. Am. Chem. Soc.* **2020**, *142*, 3296; c) C. Chen, M. Poppe, S. Poppe, C. Tschierske, F. Liu, *Angew. Chem., Int. Ed.* **2020**, *59*, 20820.
- [24] A. M. Levelut, M. Clerc, *Liqu. Cryst.* **1998**, *24*, 105.
- [25] a) X. B. Zeng, G. Ungar, M. Imperor-Clerc, *Nat. Mater.* **2005**, *4*, 562. b) X. Zeng, L. Cseh, G. H. Mehl, G. Ungar, *J. Mater. Chem.* **2008**, *18*, 2953.
- [26] a) K. Saito, Y. Yamamura, Y. Miwa, S. Kutsumizu, *Phys. Chem. Chem. Phys.* **2016**, *18*, 3280. b) N. Vaupotic, M. Salamonczyk, J. Matraszek, M. Vogrin, D. Pocięcha, E. Gorecka, *Phys. Chem. Chem. Phys.* **2020**, *22*, 12814.
- [27] a) C. Dressel, F. Liu, M. Prehm, X. B. Zeng, G. Ungar, C. Tschierske, *Angew. Chem., Int. Ed.* **2014**, *53*, 1115; b) M. Alaasar, S. Poppe, Q. Dong, F. Liu, C. Tschierske, *Chem. Commun.* **2016**, *52*, 13869.

- [28] T. Reppe, C. Dressel, S. Poppe, C. Tschierske, *Chem. Commun.* **2020**, 56, 711.
- [29] C. Dressel, T. Reppe, S. Poppe, M. Prehm, H. Lu, X. Zeng, G. Ungar, C. Tschierske, *Adv. Funct. Mater.* **2020**, *30*, 2004353.
- [30] T. Reppe, S. Poppe, X. Cai, Y. Cao, F. Liu, C. Tschierske, *Chem. Sci.* **2020**, *11*, 5902.
- [31] T. Reppe, S. Poppe, C. Tschierske, *Chem. - Eur. J.* **2020**, *26*, <https://doi.org/10.1002/chem.202002869>.
- [32] a) C. Tschierske, *Liqu. Cryst.* **2018**, *45*, 2221; b) C. Tschierske, G. Ungar, *ChemPhysChem* **2016**, *17*, 9.
- [33] H. J. Lu, X. B. Zeng, G. Ungar, C. Dressel, C. Tschierske, *Angew. Chem., Int. Ed.* **2018**, *57*, 2835.
- [34] a) C. Dressel, T. Reppe, M. Prehm, M. Brautzsch, C. Tschierske, *Nat. Chem.* **2014**, *6*, 971; b) C. Dressel, W. Weissflog, C. Tschierske, *Chem. Commun.* **2015**, 51, 15850.
- [35] M. Alaasar, M. Prehm, Y. Cao, F. Liu, C. Tschierske, *Angew. Chem., Int. Ed.* **2016**, *55*, 312.
- [36] M. Alaasar, S. Poppe, Q. Dong, F. Liu, C. Tschierske, *Angew. Chem., Int. Ed.* **2017**, *56*, 10801.
- [37] a) J. M. Wolska, J. Wilk, D. Pocięcha, J. Mieczkowski, E. Gorecka, *Chem. - Eur. J.* **2017**, *23*, 6853; b) H. R. Brand, H. Pleiner, *Eur. Phys. J. E* **2019**, *42*, 142.
- [38] S. Kutsumizu, S. Miisako, Y. Miwa, M. Kitagawa, Y. Yamamura, K. Saito, *Phys. Chem. Chem. Phys.* **2016**, *18*, 17341.
- [39] X. B. Zeng, G. Ungar, *J. Mater. Chem. C* **2020**, *8*, 5389.
- [40] A. Guijarro, M. Yus, *The Origin of Chirality in the Molecules of Life*, RSC, Cambridge, UK **2009**.
- [41] J. Buchs, L. Vogel, D. Janietz, M. Prehm, C. Tschierske, *Angew. Chem., Int. Ed.* **2017**, *56*, 280.
- [42] C. Tschierske, C. Dressel, *Symmetry* **2020**, *12*, 1098.
- [43] a) J. Barbera, E. W. Diaz, M. R. Dahrouch, E. Y. Elgueta, M. L. Parra, *Supramol. Chem.* **2014**, *26*, 373; b) Y. Sun, Y.-X. Wang, M. Wu, W. Yuan, Y. Chen, *Chem. Asian J.* **2017**, *12*, 52.
- [44] A. Escande, L. Guénée, E. Terazzi, T. B. Jensen, H. Nozary, C. Piguet, *Eur. J. Inorg. Chem.* **2010**, 2746.
- [45] J. H. Wild, K. Bartle, M. O'Neill, S. M. Kelly, R. P. Tuffin, *Liq. Cryst.* **2006**, *33*, 635.
- [46] G. S. Lim, B. M. Jung, S. J. Lee, H. H. Song, C. Kim, J. Y. Chang, *Chem. Mater.* **2007**, *19*, 460.
- [47] a) A. Kotlewski, W. F. Jager, E. Mendes, S. J. Picken, *Liq. Cryst.* **2010**, *37*, 579; b) A. Sautter, C. Thalacker, F. Würthner, *Angew. Chem., Int. Ed.* **2001**, *40*, 4425.
- [48] U. Beginn, G. Lattermann, *Mol. Cryst. Liq. Cryst.* **1994**, *241*, 215.
- [49] M. Imperor-Clerc, P. Sotta, M. Veber, *Liq. Cryst.* **2000**, *27*, 1001.
- [50] C. Destrade, N. H. Tinh, *Mol. Cryst. Liq. Cryst.* **1988**, *159*, 163.
- [51] X. Wang, C. M. Cho, W. Y. Say, A. Y. X. Tan, C. He, H. S. O. Chan, J. Xu, *J. Mater. Chem.* **2011**, *21*, 5248.
- [52] M. Alaasar, S. Poppe, Y. Cao, C. Chen, F. Liu, C. Zhu, C. Tschierske, *J. Mater. Chem. C* **2020**, *8*, 12902.
- [53] H. Li, S. S. Babu, S. T. Turner, D. Neher, M. J. Hollamby, T. Seki, S. Yagai, Y. Deguchi, H. Möhwal, T. Nakanishi, *J. Mater. Chem. C* **2013**, *1*, 1943.
- [54] The expression “swallow-tailed” was originally coined for rod-like molecules having a branched terminal chain with two branches of (almost) equal length in the terminal chains, examples are the benzylidene malonates reported in ref. [55], with a molecular shape and orientation of the alkyl chains being in some respect similar to that provided by the 3,5-disubstitution pattern at the terminal benzene ring. However, the swallow-tailed 3,5-disubstituted polycatenars have the chains directly attached to the rod-like core.
- [55] W. Weissflog, A. Wiegelegen, S. Diele, D. Demus, *Cryst. Res. Technol.* **1984**, *19*, 583.
- [56] In all cases, with one exception (compound **B6/6a**) all alkyl chain are attached via an ether oxygen to the core unit, that is, the substituents represent alkoxy groups, though for simplicity “alkyl chain” or “chains” is used throughout this manuscript.
- [57] a) G. Heppke, D. Löttsch, D. Demus, S. Diele, K. Jahn, H. Zschke, *Mol. Cryst. Liq. Cryst.* **1991**, *208*, 9; b) G. Heppke, D. Löttsch, N. K. Sharma, D. Demus, S. Diele, K. Jahn, M. Neundorf, *Mol. Cryst. Liq. Cryst.* **1994**, *241*, 275.
- [58] The structure of this SmM\*/SmM phase is not clear, especially as no aligned samples have yet been obtained for this phase.<sup>[57]</sup>
- [59] J. M. Seddon, in *Handbook of Liquid Crystals* (Eds: D. Demus, J. Goodby, G. W. Gray, H.-W. Spies, V. Vill), Wiley VCH, Weinheim, Germany **1998**, pp. 636–679.
- [60] G. W. Gray, J. W. G. Goodby, *Smectic Liquid Crystals – Textures and Structures*, L. Hill, Philadelphia, PA **1984**.
- [61] a) P. A. C. Gane, A. J. Leadbetter, P. G. Wrighton, *Mol. Cryst. Liq. Cryst.* **1981**, *66*, 247; b) J. J. Benattar, F. Moussa, M. Lambert, *J. Phys. Lett.* **1981**, *42*, 67.
- [62] S. Diele, D. Lose, H. Kruth, G. Pelzl, F. Guittard, A. Cambon, *Liq. Cryst.* **1996**, *21*, 603.
- [63] a) B. I. Ostrovskii, S. N. Sulyanov, N. I. Boiko, V. P. Shibaev, *Liq. Cryst.* **1998**, *25*, 153; b) N. Koshimizu, Y. Aizawa, K. Sakajiri, K. Shikinaka, K. Shigehara, S. Kang, M. Tokita, *Macromolecules* **2015**, *48*, 3653.
- [64] a) X.-H. Liu, B. Henrich, I. Manners, D. Guillon, D. W. Bruce, *J. Mater. Chem.* **2000**, *10*, 637; b) S. Gierlotka, J. Przedmojski, B. Pura, *Liq. Cryst.* **1988**, *3*, 1535.
- [65] Compound **B6/4** with the shortest 4'-alkoxy chain shows an additional small range of a nematic (N) phase at highest temperature (Figure S12a,b, Supporting Information). The N phase is also found for **B6/5** over a very short temperature range of <1 K on cooling and is removed for **B6/6**, which has exclusively the SmC<sub>a</sub> phase, in this case occurring below an Iso<sub>1</sub><sup>[61]</sup> phase (see Section 3.8).
- [66] a) J. Lagerwall, F. Giesselmann, *ChemPhysChem* **2006**, *7*, 20; b) H. Takezoe, E. Gorecka, M. Čepič, *Rev. Mod. Phys.* **2010**, *82*, 897; c) A. Fukuda, Y. Takanishi, T. Isozaki, K. Ishikawa, H. Takezoe, *J. Mater. Chem.* **1994**, *4*, 997.
- [67] a) S. Lagerwall, A. Dahlgren, P. Jägemalm, P. Rudquist, K. D'havØ, H. Pauwels, R. Dabrowski, W. Drzewinski, *Adv. Funct. Mater.* **2001**, *11*, 87; b) P. Perkowski, Z. Rasezewski, W. Piecek, J. Kedzierski, J. Rutkowska, J. Zielinski, X. W. Sun, *Opto-Electron. Rev.* **2011**, *19*, 34.
- [68] Y. Takanishi, H. Takezoe, A. Fukuda, H. Komura, J. Watanabe, *J. Mater. Chem.* **1992**, *2*, 71.
- [69] a) I. Nishiyama, J. W. Goodby, *J. Mater. Chem.* **1992**, *2*, 1015; b) Y. Ouchi, Y. Yoshioka, H. Ishii, K. Seki, M. Kitamura, R. Noyori, Y. Takanishi, I. Nishiyama, *J. Mater. Chem.* **1995**, *5*, 2297; c) J. Thisayukta, E. T. Samulski, *J. Mater. Chem.* **2004**, *14*, 1554; d) S.-L. Wu, F.-D. Chen, *Liq. Cryst.* **2004**, *31*, 607; e) W. Drzewinski, R. Dabrowski, K. Czupryński, J. Przedmojski, M. Neubert, *Ferroelectrics* **1998**, *212*, 281; f) K.-T. Kang, S. K. Lee, C. W. Park, S. H. Cho, J. G. Lee, S.-K. Choi, Y. B. Kim, *Bull. Korean Chem. Soc.* **2006**, *27*, 1364.
- [70] a) P. Mach, R. Pindak, A.-M. Levelut, P. Barois, H. T. Nguyen, C. C. Huang, L. Furenid, *Phys. Rev. Lett.* **1998**, *81*, 1015; b) H. F. Gleeson, L. S. Hirst, *ChemPhysChem* **2006**, *7*, 321.
- [71] a) T. Hegmann, J. Kain, S. Diele, G. Pelzl, C. Tschierske, *Angew. Chem., Int. Ed.* **2001**, *40*, 887; b) R. Pratibha, N. V. Madhusudana, B. K. Sadashiva, *Science* **2000**, *288*, 2184; c) V. Yelamaggad, I. S. Shashikala, V. P. Tamilenthir, D. S. S. Rao, G. G. Nair, S. K. Prasad, *J. Mater. Chem.* **2008**, *18*, 2096; d) B. K. Sadashiva, R. A. Reddy, R. Pratibha, N. V. Madhusudana, *Chem. Commun.*



- 2001, 20, 2140; e) K. Kishikawa, T. Inoue, Y. Sasaki, S. Aikyo, M. Takahashi, S. Kohmoto, *Soft Matter* **2011**, 7, 7532.
- [72] R. Pratihba, N. V. Madhusudana, B. K. Sadashiva, *Eur. Phys. Lett.* **2007**, 80, 46001.
- [73] H. R. Brand, P. E. Cladis, H. Pleinert, *Macromolecules* **1992**, 225, 7223.
- [74] M. A. Glaser, N. A. Clark, *Phys. Rev. E* **2002**, 66, 021711.
- [75] J. P. Wagner, P. R. Schreiner, *Angew. Chem., Int. Ed.* **2015**, 54, 12274.
- [76] Associated with the phase transition is the occurrence of weak 2nd and 3rd order layer reflections with the 3rd order being more intense than the 2nd order, representing a typical feature of the increasing sharpness of the layers in the hexatic LC phases (Figures S23 and S25, Supporting Information).
- [77] M. Neundorf, Ph.D. Thesis, Martin Luther University Halle-Wittenberg **1993**, pp. 56–59.
- [78] G. Albertini, S. Melone, G. Poeti, F. Rustichelli, G. Torquati, *Mol. Cryst. Liq. Cryst.* **1984**, 104, 121.
- [79] a) M. Deutsch, *Phys. Rev. A* **1991**, 44, 8264; b) P. Davidson, D. Petermann, A. Levelut, *A. J. Phys. II* **1995**, 5, 113.
- [80] C. Even, M. Imperor-Clerc, P. Pieranski, *Eur. Phys. J. E* **2006**, 20, 89.
- [81] Besides the major optical and X-ray scattering investigation methods used here, cubic phases have in some cases also been characterized by means of soft resonance X-ray scattering<sup>[83]</sup> and imaging methods, like AFM and TEM, especially for the larger structures of polymers, dendrimers and in cubosomes,<sup>[14,15,18–21]</sup> and the dynamics was occasionally studied by NMR experiments;<sup>[94]</sup> investigation of the faceting of cubic single crystals, slowly grown from solutions or melts, allows confirmation of the crystallographic space group.<sup>[80]</sup>
- [82] A. H. Schoen, *Interface Focus* **2012**, 2, 658.
- [83] a) Y. Cao, M. Alaasar, A. Nallapaneni, M. Salamonczyk, P. Marinko, E. Gorecka, C. Tschierske, F. Liu, N. Vaupotic, C. Zhu, *Phys. Rev. Lett.* **2020**, 125, 027801; b) Y. Cao, C. Feng, A. Jakli, C. Zhu, F. Liu, *Giant* **2020**, 2, 100018.
- [84] M. Vogrin, N. Vaupotic, M. Wojcik, J. Mieczkowski, K. Madrak, D. Pocięcha, E. Gorecka, *Phys. Chem. Chem. Phys.* **2014**, 16, 16067.
- [85] a) D. Demus, D. Marzotko, N. K. Sharma, A. Wiegeleben, *Kryst. Tech.* **1980**, 15, 331; b) A.-M. Levelut, B. Donnio, D. W. Bruce, *Liq. Cryst.* **1997**, 22, 753.
- [86] A.-M. Levelut, E. Hallouin, D. Bennemann, G. Heppke, D. Löttsch, *J. Phys. II* **1997**, 7, 981.
- [87] B. Pansu, Y. Nastishin, M. Imperor-Clerc, M. Veber, H. T. Nguyen, *Eur. Phys. J. E* **2004**, 15, 225.
- [88] a) J.-H. Ryu, M. Lee, in *Structure and Bonding*, Vol. 128 (Ed: T. Kato), Springer-Verlag, Berlin Heidelberg **2008**, pp. 63–98; b) L.-Y. Shi, Y. Zhou, X.-H. Fan, Z. Shen, *Macromolecules* **2013**, 46, 5308.
- [89] J. Kain, S. Diele, G. Pelzl, C. Lischka, W. Weissflog, *Liq. Cryst.* **2000**, 27, 11.
- [90] a) L. Rayleigh, *Proc. London Math. Soc.* **1879**, 10, 4; b) A. Eremin, U. Kornek, S. Stern, R. Stannarius, F. Araoka, H. Takezoe, H. Nadasi, W. Weissog, A. Jakli, *Phys. Rev. Lett.* **2012**, 109, 017801.
- [91] M. A. Durán-Olivencia, R. S. Gvalani, S. Kalliadasis, G. A. Pavliotis, *J. Stat. Phys.* **2019**, 174, 579.
- [92] M. K. Srinatha, S. Poppe, G. Shanker, M. Alaasar, C. Tschierske, *J. Mol. Liq.* **2020**, 317, 114244.
- [93] N. Sebastian, M.-G. Tamba, R. Stannarius, M. R. de la Fuente, M. Salamonczyk, G. Cukrov, J. Gleeson, S. Sprunt, A. Jáklí, C. Welch, Z. Ahmed, G. H. Mehl, A. Eremin, *Phys. Chem. Chem. Phys.* **2016**, 18, 19299.
- [94] a) A. Gradišek, M. Cifelli, M. Wojcik, T. Apih, S. V. Dvinskikh, E. Gorecka, V. Domenici, *Crystals* **2019**, 9, 178; b) O. Söderman, U. Henriksson, *Langmuir* **2020**, 36, 5927.
- [95] H. R. Brand, H. Pleiner, *Eur. Phys. J. E* **2017**, 40, 34.
- [96] G. M. Barretto, P. J. Collings, D. Bennemann, D. Löttsch, G. Heppke, *Liq. Cryst.* **2001**, 28, 629.
- [97] a) J. W. Goodby, D. A. Dunmur, P. J. Collings, *Liq. Cryst.* **1995**, 19, 703; b) M. Manai, A. Gharbi, J. P. Marcerou, H. T. Nguyen, J. C. Rouillon, *Physica B* **2005**, 368, 168.
- [98] O. Henrich, K. Stratford, M. E. Cates, D. Marenduzzo, *Phys. Rev. Lett.* **2011**, 106, 107801.
- [99] M. Cifelli, V. Domenici, *Phys. Chem. Chem. Phys.* **2007**, 9, 1202.
- [100] a) R. Kurita, H. Tanaka, *J. Phys. Cond. Mat.* **2005**, 17, L293; b) H. Tanaka, *Eur. Phys. J. E* **2012**, 35, 113; c) F. Sciortino, S. Mossa, E. Zaccarelli, P. Tartaglia, *Phys. Rev. Lett.* **2004**, 93, 055701; d) Y. Zhuang, K. Zhang, P. Charbonneau, *Phys. Rev. Lett.* **2016**, 116, 098301; e) M. A. Anisimov, M. Duska, F. Caupin, L. E. Amrhein, A. Rosenbaum, R. J. Sadus, *Phys. Rev. X* **2018**, 8, 011004.
- [101] A. A. Hyman, C. A. Weber, F. Jülicher, *Annu. Rev. Cell. Dev. Biol.* **2014**, 30, 39.
- [102] It is also interesting to note that upon increasing  $n$  in the series  $B6/n$ , the  $Iso_{[5]}$  phase replaces the nematic phase (Table 2). Hence, it appears that there is a competition between the development of long range orientational order and helical self-assembly as the parallel packing of the molecules becomes distorted and the preferred average molecular conformation changes from rod-like to helical by chain elongation.
- [103] Compared to the related azobenzene based compounds with 3,5-disubstitution pattern at one end,<sup>[52]</sup> the smectic phases of compounds  $Bm/n$  and  $B'6/n$  have larger tilt angles. Due to the larger tilt, the tilt correlation is stronger and no indications of uniaxial smectic phases with or without helical superstructure can be found. Though HexB phases were observed in both series, the  $SmI_s$  phases of the azobenzenes are replaced by  $SmI_s^{dis}$  phases with reduced core order. Because only short hexyl chains were used for the azobenzenes, no  $SmC_s$  and I23 phases and transitions associated with these phases could be observed.